DETERMINATION OF OPTIMUM RESULTANT FORCE AND DEPTH OF ITS APPLICATION IN UNSATURATED UNSUPPORTED VERTICAL TRENCHES CONSIDERING RAINFALL INFILTRATION

by

Ashkan Shirzadi

M.Sc.E (Drilling Engineering), Amirkabir University of Technology, 2020

A Report Submitted in Partial Fulfillment
of the Requirements for the Degree of

Master of Engineering

in the Graduate Academic Unit of Civil Engineering

Supervisors: Won Taek Oh, Ph.D., Department of Civil Engineering
Othman Nasir, Ph.D., Department of Civil Engineering

Examining Board: Taylor C. Steele, Ph.D., Department of Civil Engineering
Xiomara Sanchez-Castillo, Ph.D., Department of Civil Engineering

This report is accepted by the Dean of Graduate Studies

THE UNIVERSITY OF NEW BRUNSWICK

October, 2023

ABSTRACT

This study thoroughly examines the critical assessment of active earth pressure in unsupported vertical trenches, highlighting the unique challenges presented by unsaturated soil conditions. Traditional theories like Rankine or Coulomb lack effectiveness in such scenarios, highlighting the need to consider factors such as soil type, matric suction, and rainfall. The primary objective is to estimate active earth pressure variations during rainfall events, a critical aspect in preventing sudden failures and ensuring the safety of field workers. Extensive numerical analyses using SEEP/W and SLOPE/W reveal that applying the median resultant force at 20 or 40% of the critical depth maintains factor of safety above 1.2 during prolonged rainfall. These findings provide practical insights to mitigate risks associated with the instability of unsupported vertical trenches in unsaturated soils, ultimately enhancing the overall safety for field workers engaged in such construction operations.

DEDICATION

In sincere appreciation, I dedicate this thesis to my beloved parents, whose support, sacrifices, and continuous encouragement have been the driving force behind my academic journey.

ACKNOWLEDGEMENTS

I'm deeply grateful to Dr. Won Taek Oh, my professor and mentor, for his invaluable guidance and support. His expertise improved this report, and his encouragement inspired me. Also, his role as my supervisor made everything smoother, and I consider myself fortunate to have had the opportunity to research alongside him. Furthermore, I want to express my sincere appreciation to Dr. Nasir for guiding me during my education. His support has meant a lot to me. Finally, I want to extend my thanks to my friend and classmate Bhagya for her great help in finalizing this report. She was not only a great classmate but also a fantastic support.

Table of Contents

List of Tables

List of Figures

List of Symbols, Nomenclature or Abbreviations

Abbreviations

UVT = Unsupported Vertical Trenches

FOS = Factor of Safety

GWT = Groundwater Table

IHT = Indian Head Till

SWCC = Soil-Water Characteristic Curve

SSCC = Suction Stress Characteristic Curve

VWC= Volumetric Water Content

Symbols

k = Hydraulic Conductivity

K_a = Rankine's Active Earth Pressure Coefficient

k_{sat} = Saturated Hydraulic Conductivity

γ_{sat}= Saturated Unit Weight

C = Cohesion

c'= Effective Cohesion

ϕ'= Effective Internal Friction Angle

T_s= Surface Tension

R_s= Radius of Curvature

σ = Total Stress

σ_h = Horizontal Stress

σ_h' = Effective Horizontal Stress

σ_v = Vertical Stress

σ_v' = Effective Vertical Stress

σ^s = Suction Stress

u_a = Pore Air Pressure

u_w = Pore Water Pressure

Δu = Pressure Difference

S_e = Effective Degree of Saturation

θ = Volumetric Water Content

θ_r = Residual Volumetric Water Content

θ_s = Saturated Volumetric Water Content

a, m, n = Fitting Parameters

ψ_b = Air-Entry Value

λ = Pore-Size Distribution Index

$\psi = (u_a - u_w)$ = Matric Suction

$(\sigma - u_a)$ = Net Normal Stress

$(\sigma_h - u_a)$ = Net Horizontal Stress

$(\sigma_v - u_a)$ = Net Vertical Stress

1. INTRODUCTION

1.1. Background and Problem Statement

Unsupported vertical trenches (UVT) play an essential role in the construction of pipelines, electrical lines, stormwater, etc. since the placement of these crucial infrastructure underground provides safeguards against physical damage and deterioration caused by weathering. However, it is also important to note that unsupported trenching can pose greater risks for workers due to the confined space, particularly concerning the potential trench wall collapse that could lead to workers being trapped (Jannadi 2008). According to OSHA (Occupational Safety and Health Administration), failures or cave-ins of unsupported trenches are among the most common causes of construction-related death and serious injury. Injuries can have varying consequences such as hospitalization, long-term disability, and even fatality, impacting not only the injured workers but also their families. In addition, these excavation safety accidents can also negatively impact a company's reputation, resulting in lost productivity and increased insurance costs. The fiscal year 2022 saw an unfortunate increase in fatalities resulting from trench collapses (OSHA 2022). According to the Stephen Boyd's report (deputy regional administrator of OSHA's Region 6), 39 workers in the United States died in such accidents, exceeding the previous year's figure by more than double and marking the highest number since 2017 (Philips 2023). As a result of this concerning trend, it is imperative to follow proper safety procedures in unsupported trenching to prevent accidents and deaths.

Unsupported trench failures can happen for various causes. In regions with warm and dry climates, unsaturated soils are prevalent, and trench designs typically consider the characteristics of these soils (Bajestani and Oh 2022). However, with the ongoing climate change, rainfall patterns are becoming more intense and frequent, which can cause significant decreases in the shear strength of soils and eventually lead to failure in unsupported trenches. This indicates that it is crucial to consider changing weather patterns and the effects of climate change when designing and constructing unsupported trenches to prevent accidents and injuries.

The stability of an unsupported trench is governed by the active earth pressure profile, which is essential for estimating the critical height of an unsupported trench. When soil is fully saturated, the location of the active earth pressure is typically one-third of the height of the unsupported trench. In contrast, for unsaturated or partially saturated soils, determining the location of the active earth pressure is not as straightforward as in saturated soils. This is because the matric suction and overburden pressure profiles are a function of the degree of saturation and continuously vary under rainfall events. The primary benefit of determining the depth of the resultant active thrust is that it allows for the cost-effective improvement of unsupported trench stability without the need for trench boxes. However, the process of determining the active thrust using analytical modelling can be complex and time-consuming. In this paper, an attempt is made to investigate the variation of resultant force under rainfall events and suggest the optimal depth and magnitude of resultant force that can be applied against the UVTs to improve their stability considering rainfall

infiltration. For this, a series of numerical analyses were carried out using geotechnical modeling software SLOPE/W and SEEP/W (GeoStudio 2020, Seequent Int. Ltd.).

The present study is anticipated to enhance the design of UVTs by offering valuable insights into the behavior of unsaturated vertical trenches for diverse rainfall intensities and groundwater tables (GWTs).

1.2. Objectives of the Report

This study is designed to address the challenges that can be encountered in the design of UVTs in unsaturated soils. This report focuses on the determination of optimal force and its location that would yield a factor of safety (FOS) greater than 1.2 in UVTs, considering the worst-case scenario of rainfall events. In order to achieve this goal, the subsequent objectives were formulated:

i) To understand the stability of UVTs under rainfall events.
ii) To determine the variation of positive/negative active earth pressure profile and active thrust in unsaturated UVTs for various GWTs and a rainfall intensity.
iii) To determine the resultant force based on the positive/negative active thrust and estimate the variation of FOS by applying the resultant force along the depth of UVT.
iv) To suggest an approach that can be used for safe trenching operations without using trench boxes in practice.

Anticipated outcomes from this report include valuable insights into the behavior of UVTs, which will contribute to the improvement of design practices for such trenches in unsaturated soils.

1.3. Scope of the Report

In this study, it was assumed that the trenches were excavated into a glacial till (Indian Head till, IHT) that is widely spread across Canada. The stability and seepage analyses were carried out using the geotechnical modeling software, SLOPE/W and SEEP/W (GeoStudio 2020, Seequent Ltd.), respectively. The critical heights of UVTs were estimated for four different GWTs (i.e., 1.1, 1.4, 2.5, and 3.6 m) using SLOPE/W extending the limit equilibrium method (i.e., Bishop's simplified method). The positive and negative (i.e., matric suction) pore-water pressure distribution with depth was achieved based on the seepage analysis from SEEP/W considering the rainfall infiltration. The rainfall intensity equals to the saturated hydraulic conductivity of ITH was used in seepage analyses to consider the worst-case scenario. The methodology proposed by Shahrokhabadi et al. (2019) was adopted to establish the positive and negative active earth pressure profiles, which contribute to the instability and stability of unsupported trench, respectively. For the purpose of simplicity, the positive and negative active thrusts were calculated by extending the trapezoidal rule, which was in turn used to estimate the resultant force.

1.4. Organization of the Report

This report includes a total of six chapters, each contributing to the overall understanding of the research topic. The other chapters, in addition to the introduction provided in this initial chapter, are as follows:

- Chapter 1 includes an introduction, problem statement, and outlines the scope of the study. It offers an overview of UVT failures, emphasizing their importance in terms of worker safety and project outcomes. Within this chapter, the study's

objectives are introduced, with a central focus on comprehending the behavior of unsaturated UVTs during rainfall events and an exploration of the various factors that impact their stability.

- Chapter 2 provides an in-depth exploration of matric suction and suction stress, encompassing detailed explanations, relevant equations, and definitions of terminologies. Additionally, the difference between soil-water characteristic curve and suction stress characteristic curve is presented.
- Chapter 3 supplies vital background and theory for the study, offering explanations of key equations related to active earth pressure, its profile, influencing factors, rainfall infiltration, and hydraulic conductivity functions.
- Chapter 4 focuses on detailing the methodology employed for the numerical modeling and outlining the key assumptions made in the report. This chapter provides the properties of soil used in the report and the step-by-step procedures taken in the numerical analyses to get the valuable outcomes, including meshing properties and boundary conditions. Additionally, it explains the process of determining the resultant force, its optimum value and location for the field conditions considered in this report.
- Chapter 5 presents a detailed analysis of the results obtained through numerical modeling. This chapter discusses the trends in active earth pressure and FOS, along with the optimal resultant force and location for each scenario. This chapter also provides an extensive exploration and interpretation of the data and findings, offering valuable insights into the behavior of UVT under different field conditions.

- Chapter 6 summarized the study's primary discoveries and transformed them into conclusive insights. In addition to the conclusions, this chapter points out potential future suggestions for improving the design and safety of UVTs.

2. MATRIC SUCTION AND SUCTION STRESS

As mentioned earlier, trenches are typically excavated into soils in a state of unsaturated condition. The mechanical properties of unsaturated soils are governed by matric suction, that is the difference between pore-air and pore-water pressure. Hence, it is fundamental to understand the concept of matric suction and its influence on the mechanical properties of unsaturated soils. In the present study, active earth pressure in unsaturated soils was estimated by utilizing suction stress that is a function of matric suction. This chapter delivers the details of matric suction and suction stress, which are main factors establish the soil-water characteristic curve and soil suction characteristic curve, respectively.

2.1. Matric Suction

An unsaturated soil consists of three phases: soil particles (solid), water (liquid), and air (gas). However, it is proposed that unsaturated soil be recognized as a four-phase material due to the existence of an air-water interface (i.e., contractile skin) (Figure 2.1).

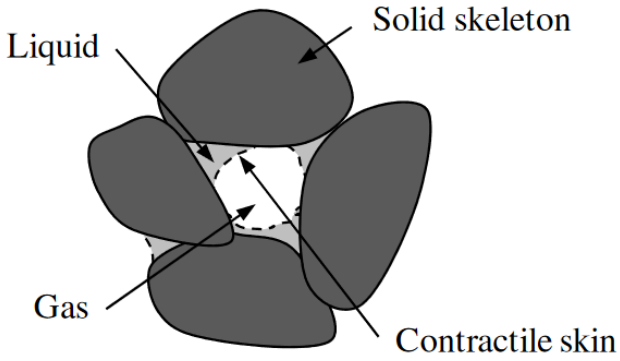

Figure 2.1. Element of unsaturated soil with bulk phases (liquid, soil skeleton, and gas) and contractile skin (Krishnapillai and Ravichandran, 2012).

For a water molecule along the contractile skin, an unbalanced force is developed towards the interior of the water body and subsequently tensile pull is generated tangentially to achieve a static equilibrium condition (Figure 2.2(a)). The property of the contractile skin that enables it to exert tensile pull is referred to as surface tension. Surface tension forms a concave curvature in the air-water interface that behaves in a manner similar to an elastic membrane (Figure 2.2(b)). The difference in pressure on the membrane is a function of surface tension and radius of curvature and can be written as Eq. (2.1) in case the radius of curvature is the same in all directions. Since the pressure difference, Δu is attributed to the difference between pore-air pressure (0-gauge pressure) and pore-water pressure (negative pressure), Eq. (2.1) can be rewritten in terms of matric suction (i.e., the difference between pore-air pressure and pore-water pressure), as shown in Eq. (2.2).

$$\Delta u = \frac{2T_s}{R_s} \tag{2.1}$$

$$u_a - u_w = \frac{2T_s}{R_s} \tag{2.2}$$

where Δu = pressure difference, T_s = surface tension, R_s = radius of curvature, u_a = pore-air pressure, u_w = pore-water pressure, and $(u_a - u_w)$ = matric suction

Eq. (2.2) demonstrates that as soil undergoes desaturation matric suction increases, resulting in a reduction in the radius of the contractile skin. This indicates that the level of matric suction is influenced by the quantity of water present within a void. This relationship can be represented by establishing the relationship between matric suction and degree of

saturation (or volumetric water content), which is referred to as the soil-water characteristic curve (SWCC, Figure 2.3). A typical SWCC consists of three main zones: boundary effect zone, transition zone, and residual zone based on air-entry value and residual suction value.

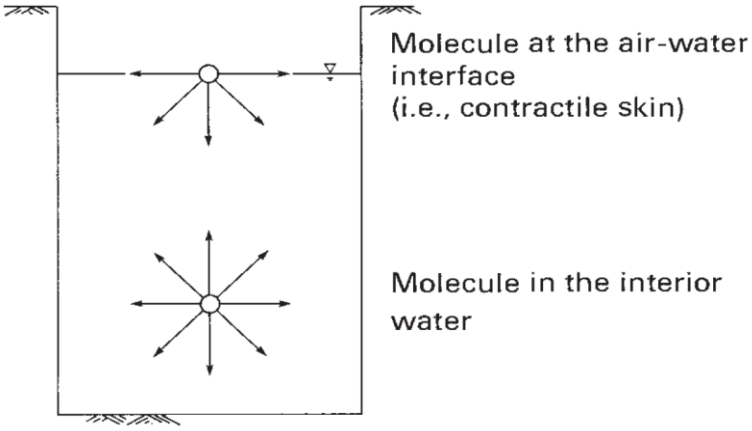

(a)

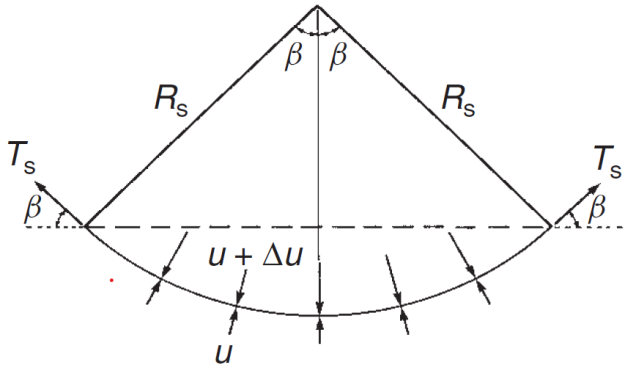

(b)

Figure 2.2. Surface tension phenomenon at air-water interface: (a) Intermolecular forces acting on contractile skin; (b) Surface tension forces associated with curved two-dimensional surface (Fredlund and Rahardjo 1993).

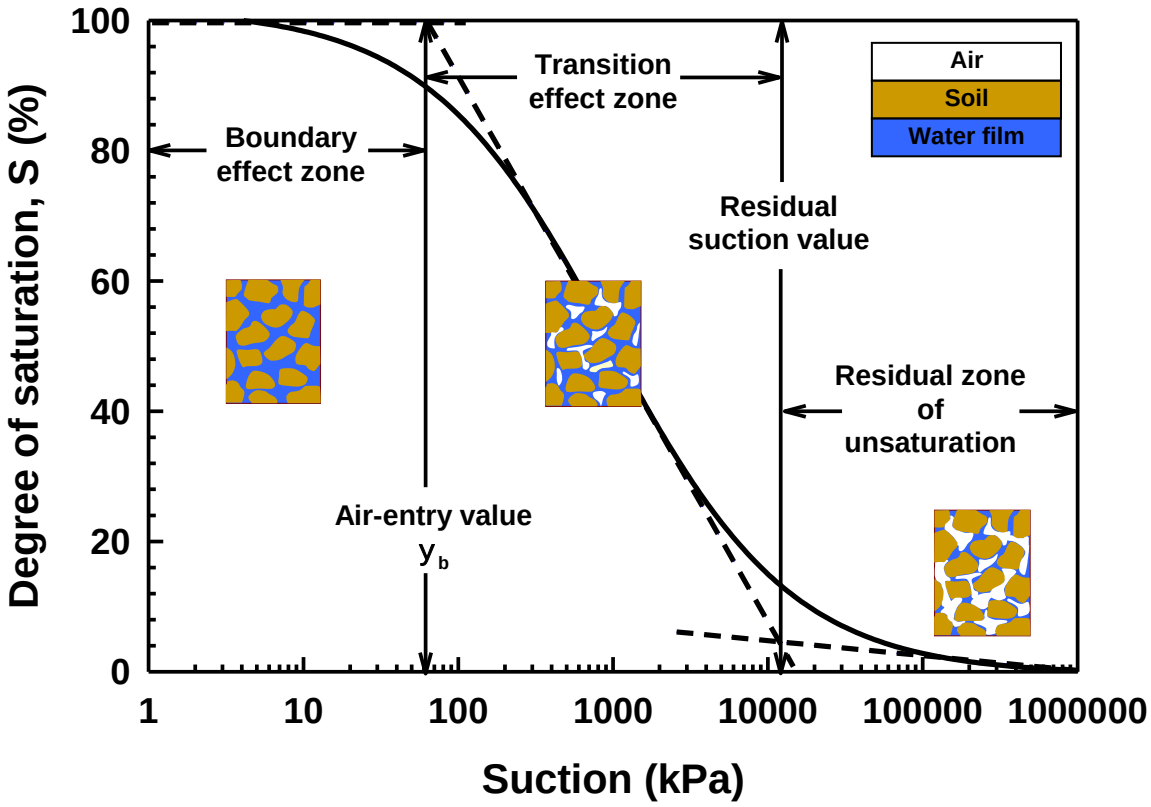

Figure 2.3. Typical SWCC showing different zones of desaturation (modified after Nishimura et al. 2008).

Matric suction plays a critical role in analyzing the behaviours of unsaturated soils since the mechanical behaviours of soil are governed by soil suction. When soil suction is less than the air-entry values (i.e., boundary effect zone), the soil retains its saturated state and exhibits behavior akin to that of saturated soil. Hence, in this zone, the shear strength of soil linearly increases with increasing the soil suction. As the suction value further increases beyond the air-entry value (i.e., transition zone), the soil starts to desaturate. The reduction in the area of water hinders the transfer of shear strength, causing a decrease in the net contribution of matric suction towards the increase in the shear strength as matric suction approaches the residual suction value. Lastly, in the residual zone of desaturation,

the contribution of soil suction toward the shear strength starts to decrease, which leads to a decrease in the shear strength (Vanapalli et al. 1996). Similar behaviours are also observed for bearing capacity and elastic modulus, as shown in Figure 2.4.

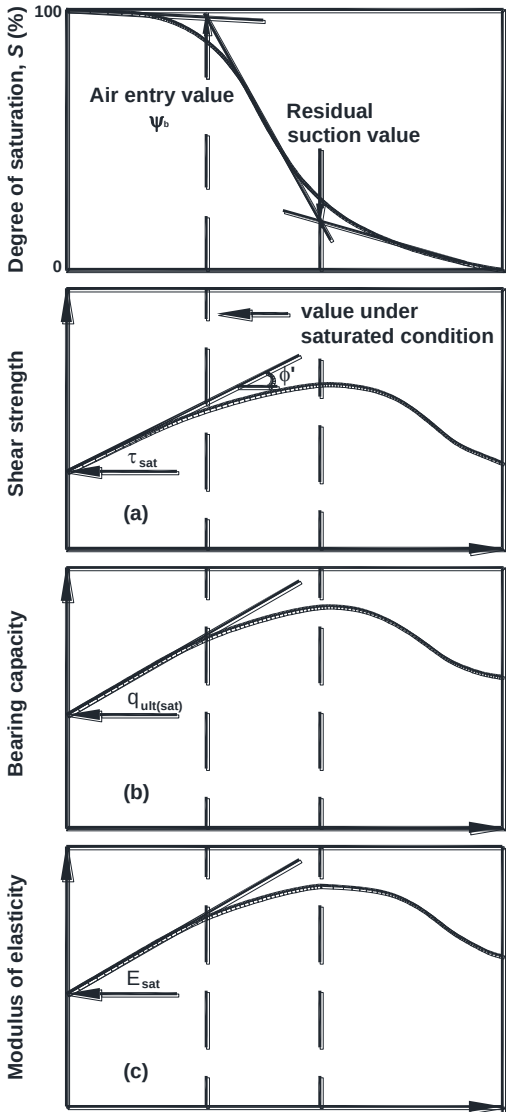

Figure 2.4. SWCC and the variation of (a) shear strength, (b) bearing capacity, and (c) modulus of elasticity with respect to matric suction (modified after Oh et al. 2009).

Determination of the SWCC through experiment is time-consuming and requires elaborate testing apparatus. Due to this reason, various SWCC fitting models have been proposed in the literature that can be used to establish the SWCC across the complete range of suction (i.e., 0 to 10^6 kPa). Some examples of SWCC best-fit models are shown in Eq. (2.3) (Brooks and Corey 1964), Eq. (2.4) (Van Genuchten 1980), and Eq. (2.5) (Fredlund and Xing 1994).

$$S_e = \frac{(\theta - \theta_r)}{(\theta_s - \theta_r)} = \begin{cases} \left(\frac{\psi}{\psi_b}\right)^{-\lambda} & \psi > \psi_b \\ 1 & \psi_b \geq \psi \end{cases} \tag{2.3}$$

$$S_e = \frac{(\theta - \theta_r)}{(\theta_s - \theta_r)} = \left[\frac{1}{1+(\alpha\psi)^{n_{vG}}}\right]^{m_{vG}} \qquad \left(m_{vG} = 1 - 1/n_{vG}\right) \tag{2.4}$$

$$\frac{\theta}{\theta_s} = \frac{C(\psi)}{\ln\left[e + (\psi/a)^{n_{FX}}\right]^{m_{FX}}};\ C(\psi) = 1 - \frac{\ln(1+\psi/C_r)}{\ln\left[1+10^6/C_r\right]} \tag{2.5}$$

where S_e = effective saturation, ψ = soil suction, ψ_b = air-entry value, λ = pore-size distribution index, α, n_{vG}, and m_{vG} = fitting parameters for Van Genuchten's (1980) model, a n_{FX}, and m_{FX} = fitting parameters for the Fredlund and Xing's (1994) model, $C(\psi)$ = correction factor, C_r = parameter related to the residual water content, e = Euler's number, θ = volumetric water content, and θ_s, θ_r = saturated and residual volumetric water contents, respectively

2.2. Suction Stress

Pore-water in soil exists in two different forms: meniscus water and bulk water (Karube and Kato 1994, Karube and Kawai 2001) (Figure 2.5). Meniscus water exists around the contact points of soil particles, while bulk water is referred to as a larger mass of pore water formed by the combination of meniscus water containing some contact points of soil particles.

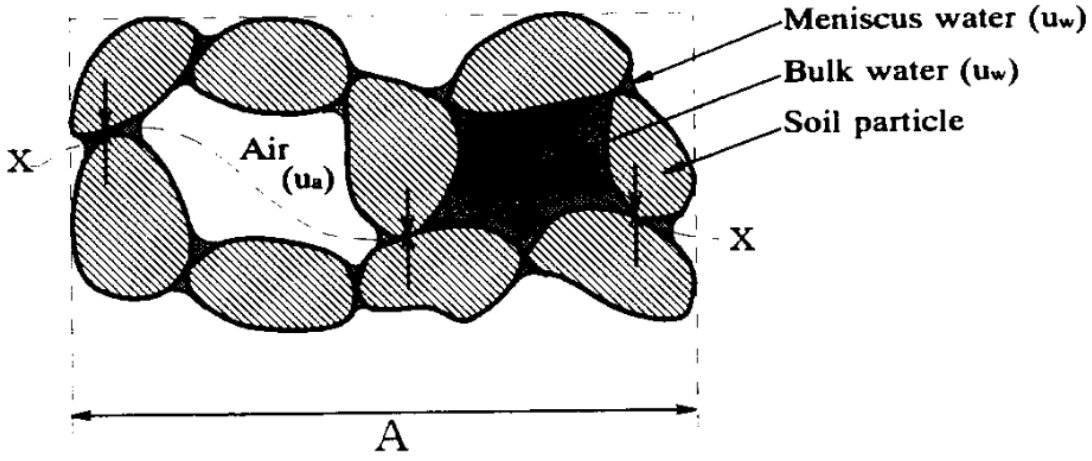

Figure 2.5. Wavy section of general unsaturated soils, showing meniscus water and bulk water (Karube and Kawai 2001).

Extending this concept, suction stress can be given by

$$\sigma^s = \sigma_m + \sigma_b \tag{2.6}$$

where σ^s = compressive stress yielded by suction (i.e., suction stress), σ_m = compressive stress yielded by meniscus water (i.e., meniscus stress), and σ_b = compressive stress yielded by bulk water (i.e., bulk stress)

The effective stress of saturated soils proposed by Terzaghi (1943) is expressed as Eq. (2.7)

.

$$\sigma' = \sigma - u_w \tag{2.7}$$

where σ' = effective stress, and σ = total stress

Bishop (1959) introduced the concept of the effective stress approach for unsaturated soils (Eq. (2.8)) by incorporating a new effective stress parameter, χ into Terzaghi's original equation for effective stress (i.e., Eq. (2.7)).

$$\sigma'_{unsat} = (\sigma - u_a) + \chi (u_a - u_w) \tag{2.8}$$

where σ'_{unsat} = effective stress for unsaturated soils, $(\sigma - u_a)$ = net normal stress, and χ = effective stress parameter that is a function of the degree of saturation, varying between zero and unity

Lu and Likos, (2004, 2006) proposed that the effective stress of unsaturated soils can be expressed in terms of suction stress, as shown in Eq. (2.9).

$$\sigma'_{unsat} = (\sigma - u_a) - \sigma^s \tag{2.9}$$

Considering Eq. (2.8) and Eq. (2.9), suction stress can be reformulated as Eq. (2.10).

$$\sigma^s = -\chi\left(u_a - u_w\right) \tag{2.10}$$

The research on the shear strength of unsaturated soils suggests that the parameter, χ can be replaced with the effective saturation (Karube et al. 1996, Vanapalli et al. 1996). Hence, Eq. (2.10) can be rewritten as Eqs. (2.11) or Eq. (2.12) depending on the suction value.

$$\sigma^s = -\left(u_a - u_w\right) \qquad if\ \left(u_a - u_w\right) < 0 \tag{2.11}$$

$$\sigma^s = -S_e\left(u_a - u_w\right) \quad if\ \left(u_a - u_w\right) \geq 0 \tag{2.12}$$

Lu et al. (2010) developed a closed-form equation that can be used to estimate the variation suction stress (Eq. (2.13)) with respect to soil suction by substituting Eq. (2.4) into Eq. (2.8) to eliminate the effective saturation.

$$\sigma^s = \left[\frac{\psi}{1+\left(\alpha\psi\right)^{n_{vG}}}\right]^{m_{vG}} \qquad \left(m_{vG} = 1 - 1/n_{vG}\right) \tag{2.13}$$

The relationship between the degree of saturation and suction stress is denoted as the suction stress characteristic curve (SSCC). Figure 2.6 shows the interrelationship between the SWCC and the SSCC. The hatched area under the SWCC indicates the graphical representation of suction stress.

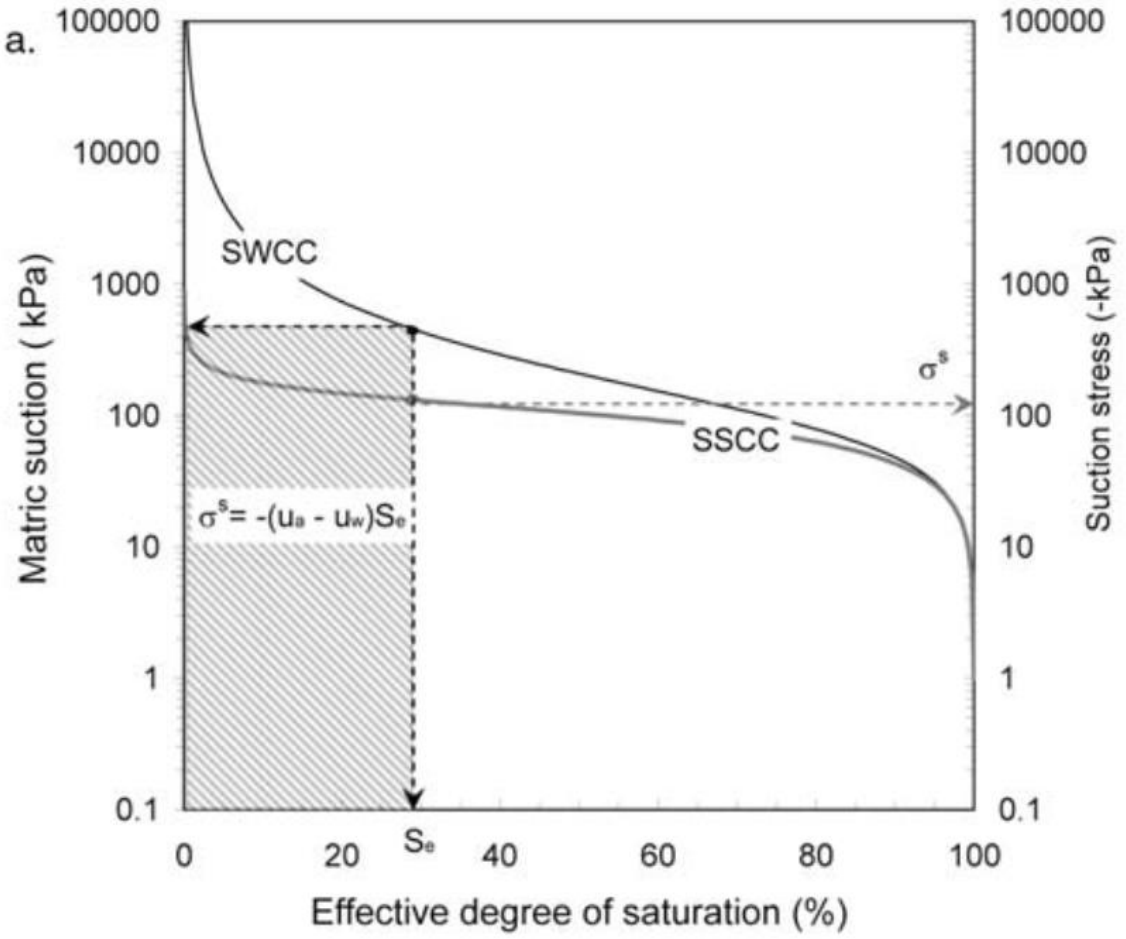

Figure 2.6. The interrelationship between the SWCC and the SSCC (Lu et al. 2010).

3. ACTIVE EARTH PRESSURE IN UNSATURATED SOILS

3.1 Calculation of Active Earth Pressure

The excavation of a UVT causes disturbance and alteration to the natural state of the surrounding soil. Consequently, an active condition is induced in the vicinity of the trench, causing the instability of UVT. The effective horizontal stress in saturated soil can be calculated using the approach proposed by Rankine (1857) (Eq. (3.1)) .

$$\sigma'_h = \sigma'_v K_a - 2c'\sqrt{K_a} \tag{3.1}$$

where σ'_h = horizontal effective pressure, c' = effective cohesion, σ'_v = vertical effective stress, ϕ'= effective internal friction angle and K_a = Rankine's active earth pressure coefficient (Eq. (3.2)).

$$K_a = \tan^2\left(45° - \frac{\phi'}{2}\right) \tag{3.2}$$

In many cases, UVTs are typically excavated into soils that are in a state of unsaturated conditions. This implies that the contribution of matric suction towards the active earth pressure should be taken into account when designing/excavating a UVT. The pioneering research on the active and passive earther pressure in a UVT was carried out by Pufahl et al. (1983). They suggested that the horizontal net normal pressure can be expressed as Eq. (3.3) by adopting the Mohr-Coulomb failure criteria and the Rankine earth pressure theory.

$$\sigma_h - u_a = (\sigma_v - u_a) K_a - 2\left[c' + (u_a - u_w) \tan \phi^b \right] \sqrt{K_a} \tag{3.3}$$

Eq. (3.3) can be rewritten as Eq. (3.4) assuming $u_a = 0$ (i.e., atmospheric pressure).

$$\sigma_h = \sigma_v K_a - 2\left[c' + (u_a - u_w) \tan \phi^b \right] \sqrt{K_a} \tag{3.4}$$

where ($\sigma_h - u_a$) = net horizontal stress, ($\sigma_v - u_a$) = net vertical stress, σ_h and σ_v = horizontal and vertical normal pressure, respectively, and ϕ^b is the angle indicating the rate of increase in shear strength with respect to a change in matric suction.

Vahedifard et al. (2015) proposed an approach that can be used to calculate the active thrust in unsaturated retaining structures' steady flow conditions. For this, the variation of active earth pressure coefficient, K_a due to the infiltration and evaporation was investigated considering various factors such as effective internal friction, air-entry pressure parameter, soil type, tension crack and interface friction angle. The research employs a closed-form equation by utilizing the suction stress-based effective stress approach, assuming a log spiral failure surface under vertical unsaturated steady seepage conditions (Figure 3.1).

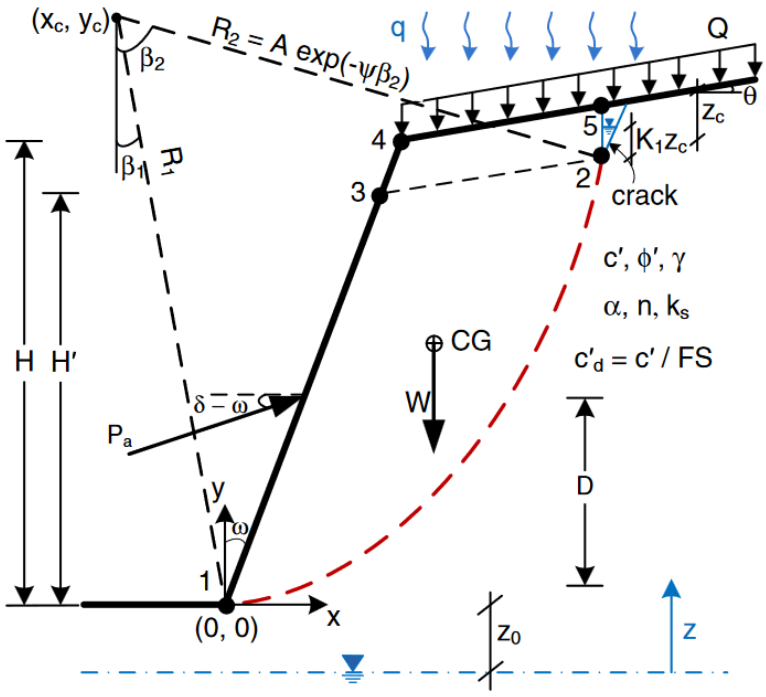

Figure 3.1. Notation/conventions and failure mechanism used by (Vahedifard et al., 2015)

The variation of suction stress due to vertical unsaturated steady seepage was calculated using Eq. (3.5).

$$\sigma_s = \frac{1}{\alpha}\frac{\ln\left[\left(1+\frac{q_v}{k_{sat}}\right)e^{-\gamma_w\alpha(z_0+y)}-\frac{q_v}{k_{sat}}\right]}{\left(1+\left\{-\ln\left[\left(1+\frac{q_v}{k_{sat}}\right)e^{-\gamma_w\alpha(z_0+y)}-\frac{q_v}{k_{sat}}\right]\right\}^n\right)^{(n-1)/n}} \tag{3.5}$$

where α, n = soil-water characteristic curve fitting parameters (van Genuchten, 1980), q_v = vertical discharge, γ_w = unit weight of water, k_{sat} = saturated hydraulic conductivity,

z_0 = constant value representing the vertical distance from the GWT to the toe of the wall, and y = distance from the toe of the wall

The proposed approach was used to estimate the influence of matric suction on the stability of the retaining wall extending the limit equilibrium method. The analysis results showed that evaporation and infiltration significantly increase and decrease active thrust, respectively. However, the influence of suction stress becomes negligible as the wall height increases mainly due to the backfill-wall friction.

Shahrokhabadi et al. (2019) proposed a methodology to estimate the horizontal stress in unsaturated soils by extending Rankine's active earth pressure theory (i.e., Eq. (3.1)). This can be obtained by incorporating Eq. (2.9) into Eq. (3.6), yielding Eq. (3.7).

$$\left(\sigma_h - u_a\right) = \left(\sigma_v - u_a\right) K_a - 2c'\sqrt{K_a} - \left(K_a - 1\right)\sigma^s \tag{3.7}$$

where σ_v, σ_h = vertical and horizontal stress, respectively

The active earth pressure in unsaturated soils, σ_a then can be estimated using Eq. (3.8), assuming atmospheric pressure (i.e., $u_a = 0$).

$$\sigma_h = \sigma_a = \sigma_v K_a - 2c'\sqrt{K_a} - \left(K_a - 1\right)\sigma^s \tag{3.8}$$

Eq. (3.8) demonstrates that the active earth pressure in an unsaturated UVT can be estimated by taking into account three crucial components: vertical stress, effective

cohesion, and suction stress. The vertical stress acts as an instability factor, contributing to positive active earth pressure, while effective cohesion and suction stress act as stabilization factors, resulting in negative active earth pressure. The influence of these factors on the trench wall is depicted in Figure 3.2. The depth of the tension zone is defined as the depth where the net horizontal stress becomes zero. The critical height (FOS =1) can be determined as a depth where the negative (i.e., Area I) and positive (i.e., Area II) active thrusts are the same.

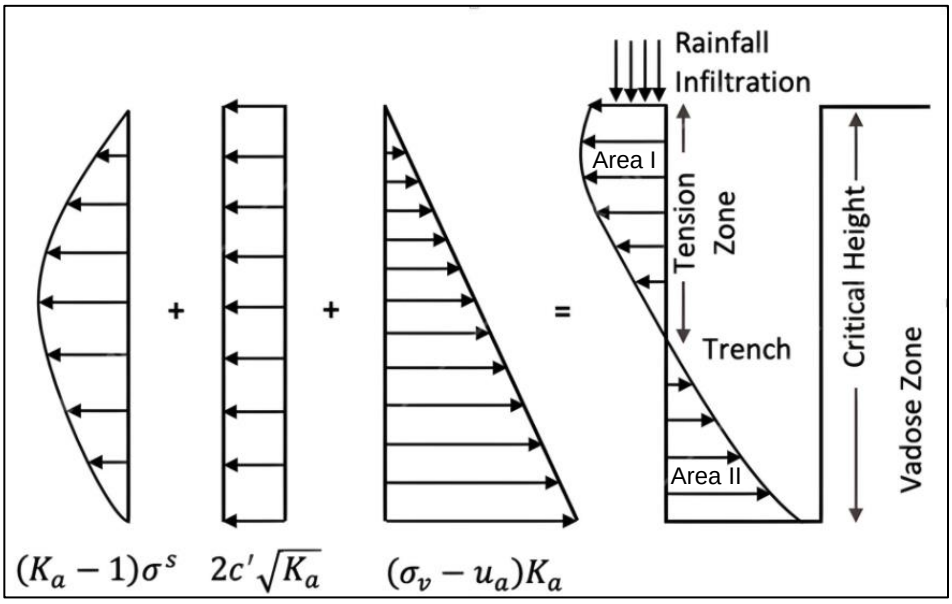

Figure 3.2. Active earth pressure profile in an unsaturated UVT (modified after Shahrokhabadi et al. 2019).

Richard et al. (2021) investigated the variation of critical heights of UVTs in coarse- and fine-grained soils with respect to the depth of GWT. The critical heights were estimated using two different approaches: namely, numerical and analytical methods. In the case of the analytical method, the active earth pressure was calculated using Eq. (3.9) by extending the approach originally proposed by Pufahl et al. (1983, Eq. (3.3)).

$$\begin{aligned}\sigma_h &= \sigma_v K_a - 2\left[c' + \left(u_a - u_w\right)\left(S^\kappa\right)\tan\phi'\right]\sqrt{K_a} \\ &= \sigma_v K_a - 2C\sqrt{K_a}\end{aligned} \tag{3.9}$$

where S = saturation, C = total cohesion, and κ = fitting parameter that is a function of plasticity index

In Eq. (3.9), The angle indicating the rate of increase in shear strength with respect to a change in matric suction (i.e., $tan\phi^b$) is replaced with Eq. (3.10) (Vanapalli et al. 1996).

$$\tan\phi^b = \left(S^\kappa\right)\tan\phi' \tag{3.10}$$

An example of the active earth pressure diagram in a UVT is shown in Figure 3.3. The critical height can be estimated by locating the depth that equates positive and negative active thrusts, where the net horizontal thrust is zero.

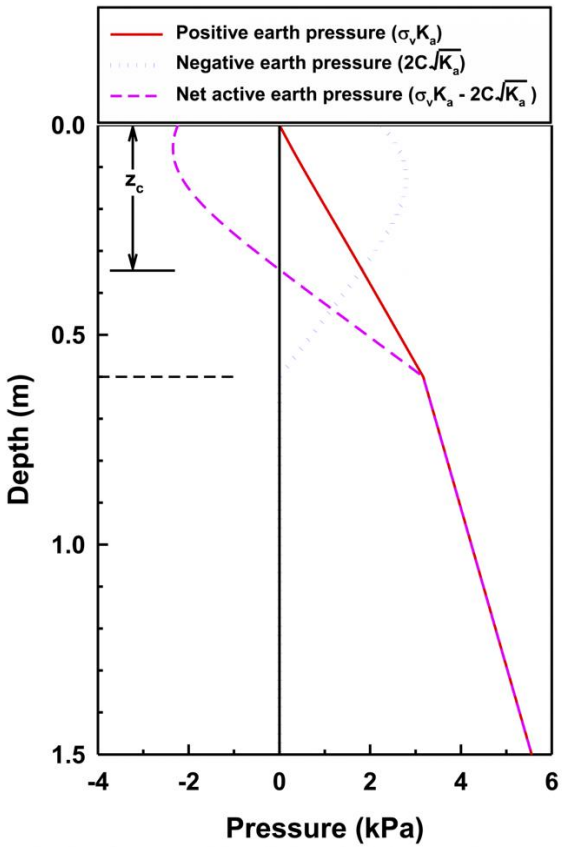

Figure 3.3. Example of active earth pressure diagram in UVT.

3.2 Rainfall Infiltration into UVTs

Rainfall infiltration reduces the contribution of suction stress towards the negative active pressure, resulting in a decrease in the depth of the tension zone. As rainfall infiltrates into UVTs, the pore-water pressure increases, leading to a reduction in suction stress. Given that suction stress plays a role in maintaining the stability of UVTs, rainfall infiltration into UVTs decreases their stability due to the decrease in the shear strength of soils. This phenomenon can be overcome effectively by applying force against the soil mass, without the use of a trench box.

In unsaturated soils, hydraulic conductivity varies with respect to soil suction, which is denoted as the hydraulic conductivity function. Hence, it is crucial to employ a suitable hydraulic conductivity function to accurately predict the changes in FOS in UVTs during rainfall events. Various hydraulic conductivity functions are available in the literature; among those, the hydraulic conductivity functions proposed by Brooks and Corey (1964), Van Genuchten (1980), and Fredlund et al. (1994), are the most commonly used.

Brooks and Corey (1964)

Brooks and Corey (1964) introduced a model that can be used to predict the hydraulic conductivity of unsaturated soils by utilizing the hydraulic conductivity for saturated conditions and the SWCC established by the SWCC fitting model proposed by Brooks and Corey (1964, Eq. (2.3)) (Eq. (3.11)).

$$k = \begin{cases} k_{sat}\left(\dfrac{\psi}{\psi_b}\right)^{2+(5\lambda/2)} & \psi > \psi_b \\ k_{sat} & \psi_b \geq \psi \end{cases} \tag{3.11}$$

where k = hydraulic conductivity of the water phase

Van Genuchten (1980)

Given the limitations of Brooks and Corey's (1964) model, rapidly converging during numerical simulations of seepage in saturated-unsaturated soils, Van Genuchten (1980) proposed an alternative model. This model provides a closed-form equation that enables

the prediction of hydraulic conductivity, which is well-suited for simulating fluid flow in scenarios involving both saturated and unsaturated soils. This model utilizes the hydraulic conductivity for saturated condition and SWCC obtained with the SWCC fitting model proposed by Van Genuchten (1980, Eq. (2.4)) (Eq. (3.12)).

$$k = k_{sat}\left[\frac{\left\{1-\left(\alpha\psi\right)^{\left(n_{vG}-1\right)}\left[1+\left(\alpha\psi\right)^{n_{vG}}\right]^{-m_{vG}}\right\}^{2}}{\left[1+\left(\alpha\psi\right)^{n_{vG}}\right]^{\left(1/2-n_{vG}/2\right)}}\right] \tag{3.12}$$

Fredlund et al. (1994)

The hydraulic conductivity model proposed by Fredlund et al. (1994) utilizes the hydraulic conductivity for saturated condition and the SWCC obtained with the SWCC best-fit model proposed by Fredlund and Xing (1994, Eq. (2.5)) (Eq.(3.13)). Unlike the Van Genuchten's (1980) model, this model is complex and does not present a closed-form solution.

$$k = k_{sat}\left\{\frac{\int_{ln(\psi)}^{b}\left(\theta\left(e^{y}\right)-\theta\left(\psi\right)\right)\Big/e^{y}\theta'\left(e^{y}\right)dy}{\int_{ln(\psi_b)}^{b}\left(\theta\left(e^{y}\right)-\theta_s\right)\Big/e^{y}\theta'\left(e^{y}\right)dy}\right\} \tag{3.13}$$

where y = dummy variable of integration representing the logarithm of the soil suction, θ' = first derivative of Eq. (2.5), and b = upper limit of integration

4. METHODOLOGY

Chapter 4 outlines the methodology employed in this study to investigate the stability of UVTs in geotechnical engineering practice, focusing on the optimization of resultant force application depth. The foundation of this report lies in understanding the physical and mechanical properties of the Indian Head till, (hereafter referred to as IHT), a glacial till that is widely spread across Canada (Oh and Vanapalli 2013, 2010). To address the influence of rainfall infiltration on UVT stability, numerical analysis using SEEP/W and SLOPE/W is conducted. The study navigates through a series of steps, including critical height determination, rainfall event simulation, active earth pressure analysis, and resultant force optimization. The methodology, as detailed in this chapter, provides a systematic approach to enhancing UVT stability, and serves as a valuable contribution to the field of soil mechanics. The flowchart of the methodology is shown in Figure 4.1.

4.1 Soil Properties

In this study, it was assumed that UVTs are excavated into IHT. The physical and mechanical properties of the samples obtained from IHT are summarized in Table 4.1.

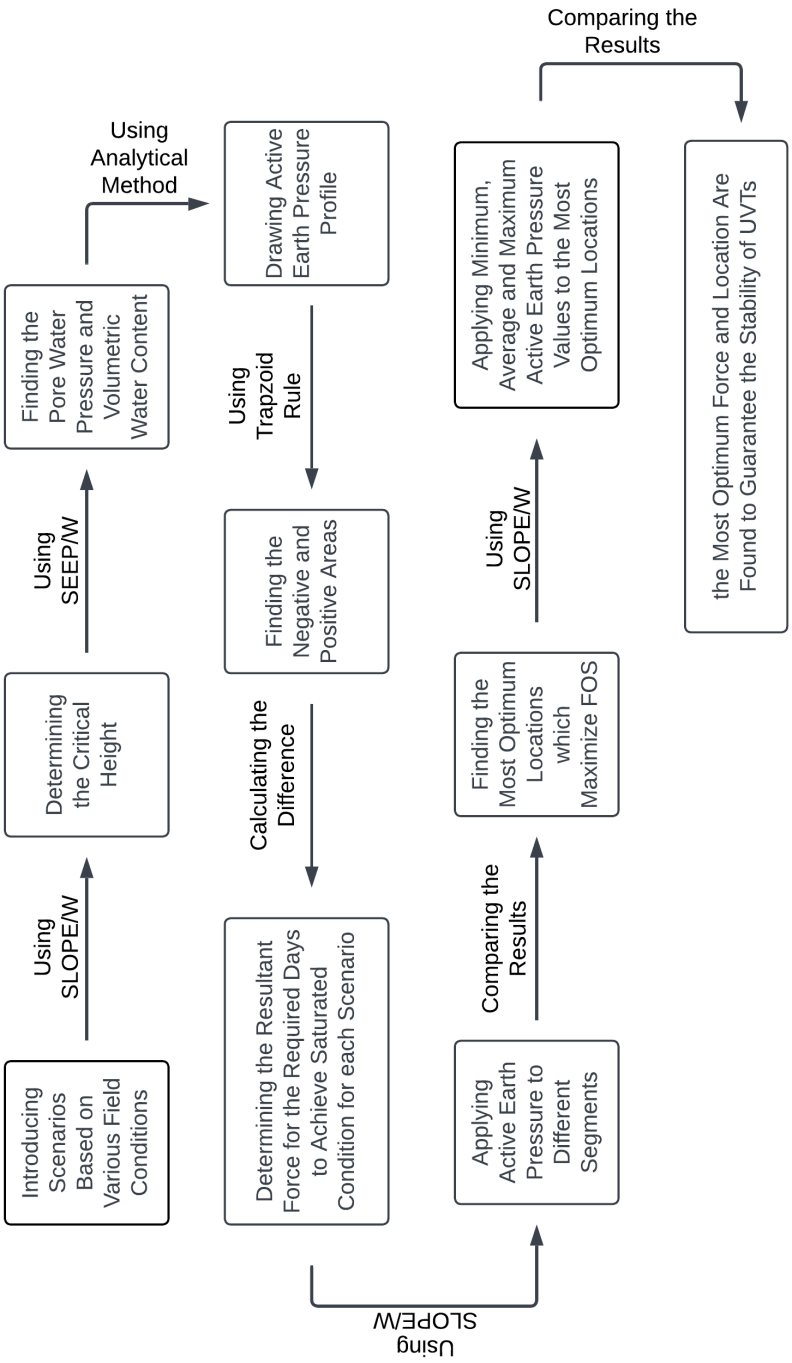

Figure 4.1. Methodology flow chart.

Table 4.1. Basic properties of IHT (Oh and Vanapalli, 2013, 2010).

Soil Property	Value
Effective cohesion, (kPa)	5
Effective internal friction angle, ϕ' (°)	23.1
Saturated unit weight, γ_{sat} (kN/m^3)	20.7
Saturated volumetric water content, θ_s	0.468
Saturated hydraulic conductivity, k_{sat} (m/sec)	10^{-7}

Figure 4.2 shows the SWCC of IHT, obtained with the fitting model proposed by Fredlund and Xing (1994, Eq. (2.5)). The hydraulic conductivity function of IHT (with the fitting parameters) was established using the model proposed by Fredlund et al. (1994, Eq. (3.12)), as shown in Figure 4.3.

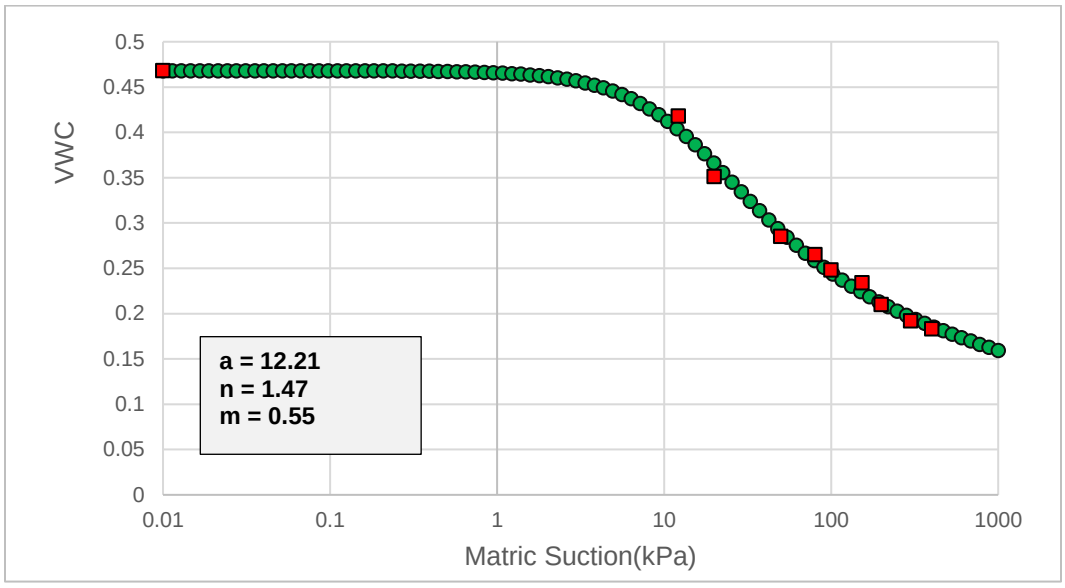

Figure 4.2. The soil-water characteristic curve of IHT.

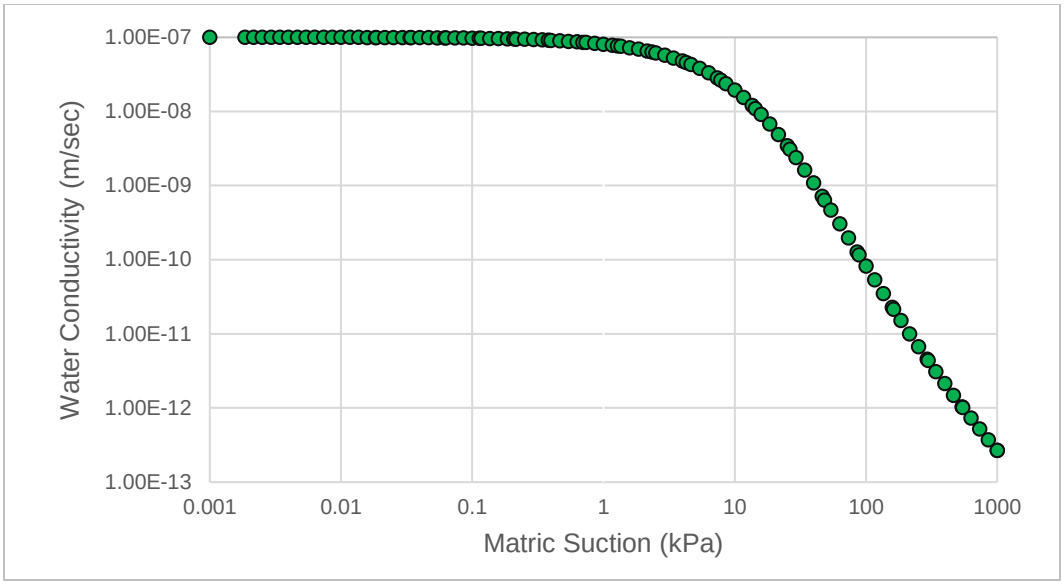

Figure 4.3. Hydraulic conductivity function of IHT.

For unsaturated soils, the shear strength is governed by matric suction; therefore, it is critical to consider the variation of shear strength with respect to suction during rainfall events. Various shear strength models are available for unsaturated soils. Among those, the shear strength model proposed by Vanapalli et al. (1996) is adopted in the present study (Eq. (4.1)).

$$\tau_{unsat} = c' + (\sigma_n - u_a)\tan\phi' + (u_a - u_w)\left[\frac{\theta - \theta_r}{\theta_s - \theta_r}\right]\tan\phi' \qquad (4.1)$$

where τ_{unsat} = shear strength of unsaturated soil, c' = effective cohesion, $(u_a - u_w)$ = matric suction, $(\sigma_n - u_a)$ = net normal stress, θ = volumetric water content, and θ_s, θ_r = saturated and residual volumetric water contents, respectively

4.2 Numerical Analysis

As previously stated, the objective of this study is to identify the optimal depth of resultant force application that would maximize the stability of UVTs considering rainfall infiltration. For this, the geotechnical modeling software, SEEP/W and SLOPE/W were jointly used for seepage and stability analysis, respectively.

Excavation in soil causes a reduction in total confining stress, which in turn leads to a swelling in the soil mass. In this case, reduction in the pore-water pressure due to excavation can be estimated using Eq. (4.2).

$$\Delta u_w = B\left[\Delta\sigma_3 + A\left(\Delta\sigma_1 - \Delta\sigma_3\right)\right] \tag{4.2}$$

where A, B = Skempton's (1954) pore-water pressure coefficients, $\Delta\sigma_3$ = change in total confining stress, and $(\Delta\sigma_1 - \Delta\sigma_3)$ = change in axial stress

Following excavation, water flows towards the slope and the pore-water pressure gradually increases with the dissipation of negative excess pore-water pressure. Therefore, FOS becomes maximum at the end of the excavation. After a certain period of time, steady seepage is achieved and the FOS declines to its lowest value (Figure 4.4). Richard et al. (2021) carried out finite element coupled stress-pore-water pressure analyses to investigate the variation of FOS with time due to unsupported trenching in unsaturated soil. As can be seen in Figure 4.5, FOS is relatively high right after the trenching due to the drop in the GWT. FOS then gradually decreases with time as the GWT rounds towards its original

level. Hence, in the present study, it was assumed that the groundwater remains unchanged during trenching to consider the worst-case scenario.

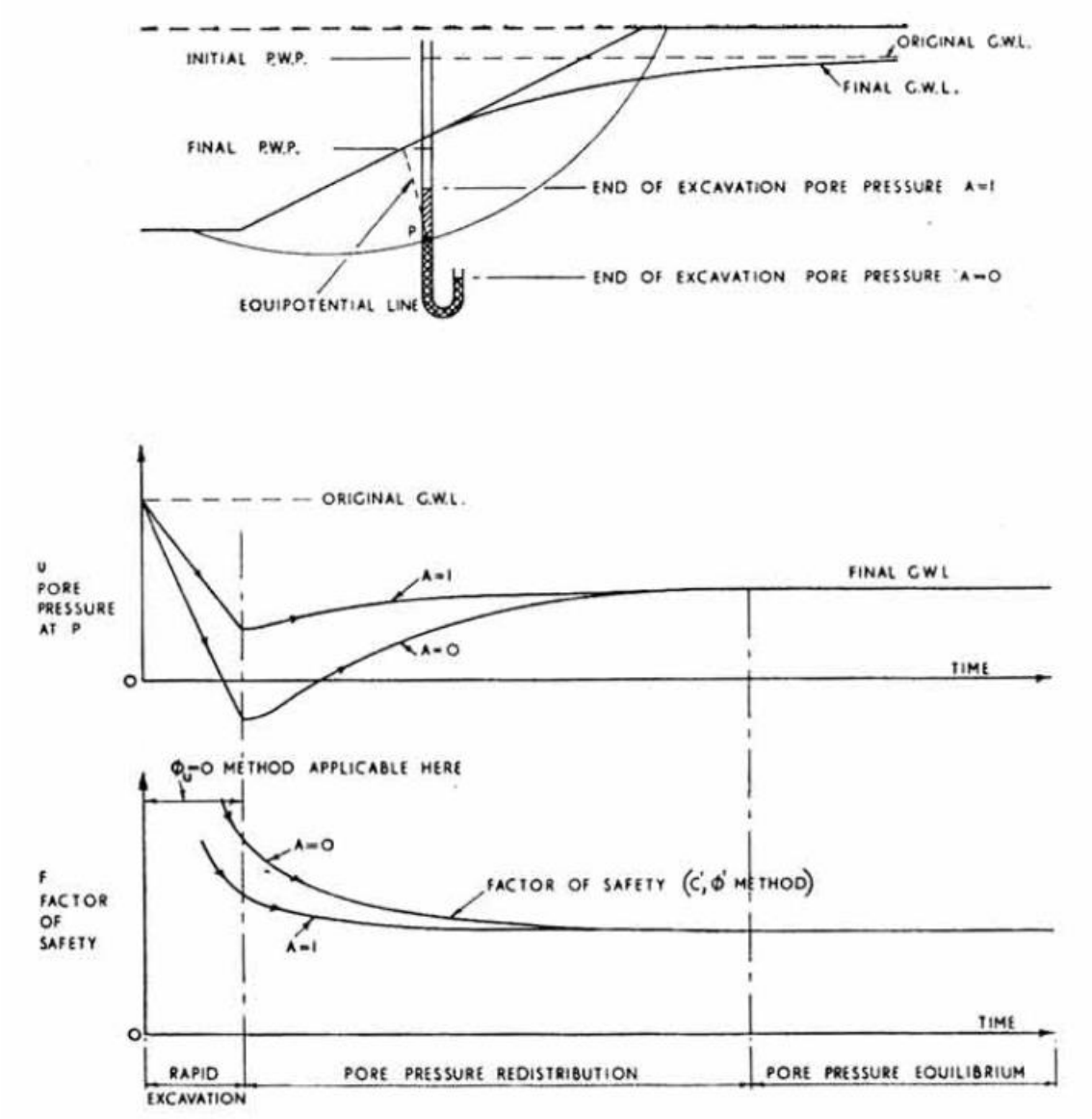

Figure 4.4. The change in pore-water pressure and factor of safety during and after the excavation of a cut in clay (Bishop and Bjerrum 1960).

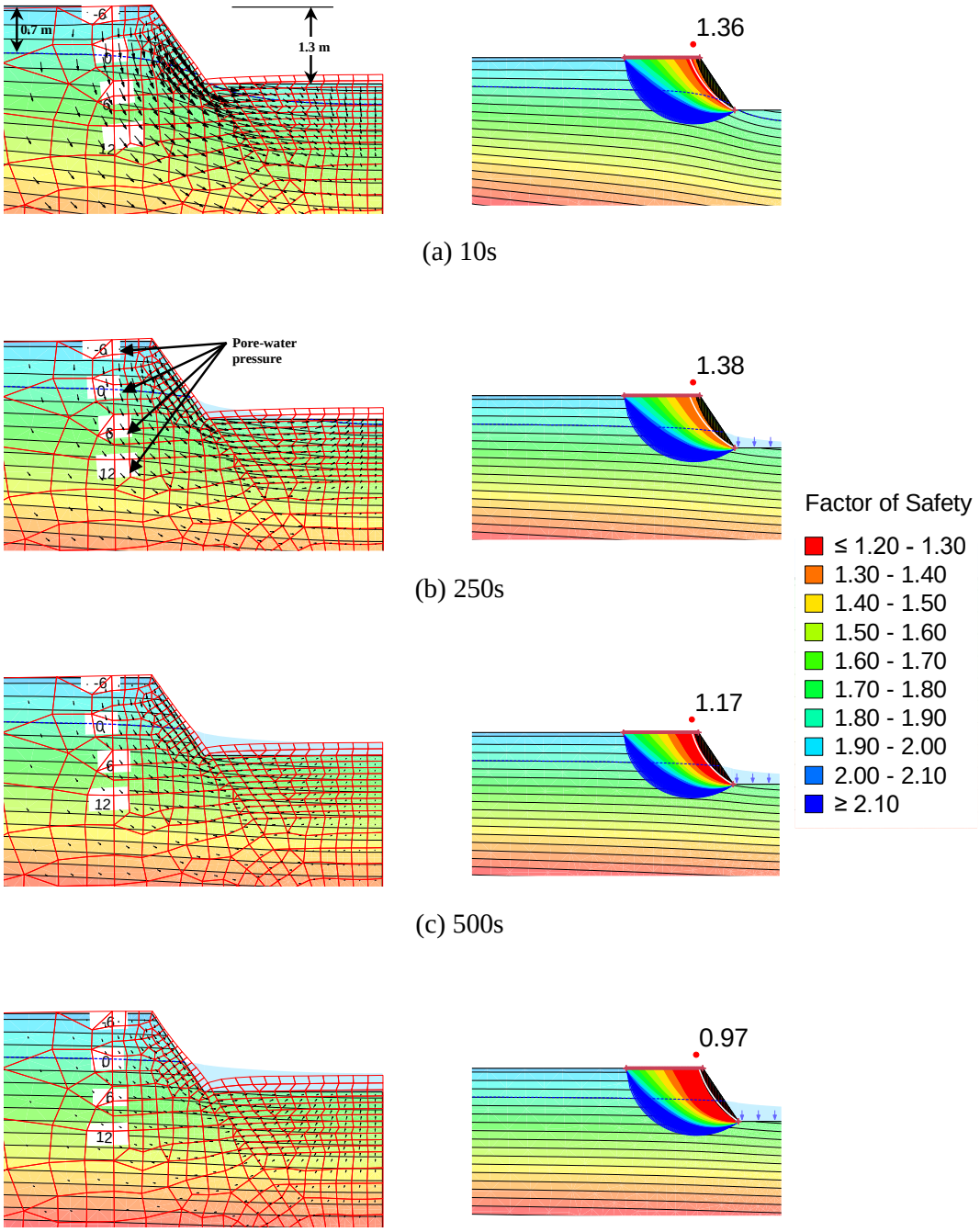

Figure 4.5. Variation of FOS with time in an unsupported trench (GWT at 0.7 m, 1.5V:1H) (Richard et al. 2021).

Analyses were carried out with GWTs at 1.1 m, 1.4 m, 2.5 m, and 3.6 m from the ground surface to simulate field conditions with low and high water levels within the UVT. Each case was denoted as Scenario I, II, III, and IV. In the case where a UVT is excavated below the GWT, the hydraulic static pressure due to the water reservoir helps to stabilize the UVT. This phenomenon can lead to a higher critical height for a UVT with a shallow GWT rather than that with a deep one (Richard et al. 2021). However, in practice, the water within a UVT is usually pumped out before construction operation. In this report, the resultant forces were calculated without considering the hydrostatic pressure for conservative analysis. The step-by-step procedures used in the numerical analyses are as follows:

Step 1: Determining the Critical Height of a UVT

Initially, the critical height (FOS = 1) of a UVT was determined using SLOPE/W for a given GWT. To achieve this goal, simulations were conducted with various trench depths for a given GWT to identify the depth at which a FOS of 1 is attained. To identify potential slip surfaces, the 'Entry and Exit' slip surface option was employed. A specific point located at the toe of the trench was chosen for the exit point, while a range was defined along the ground surface as an entry to include all possible slip surfaces (Figure 4.6).

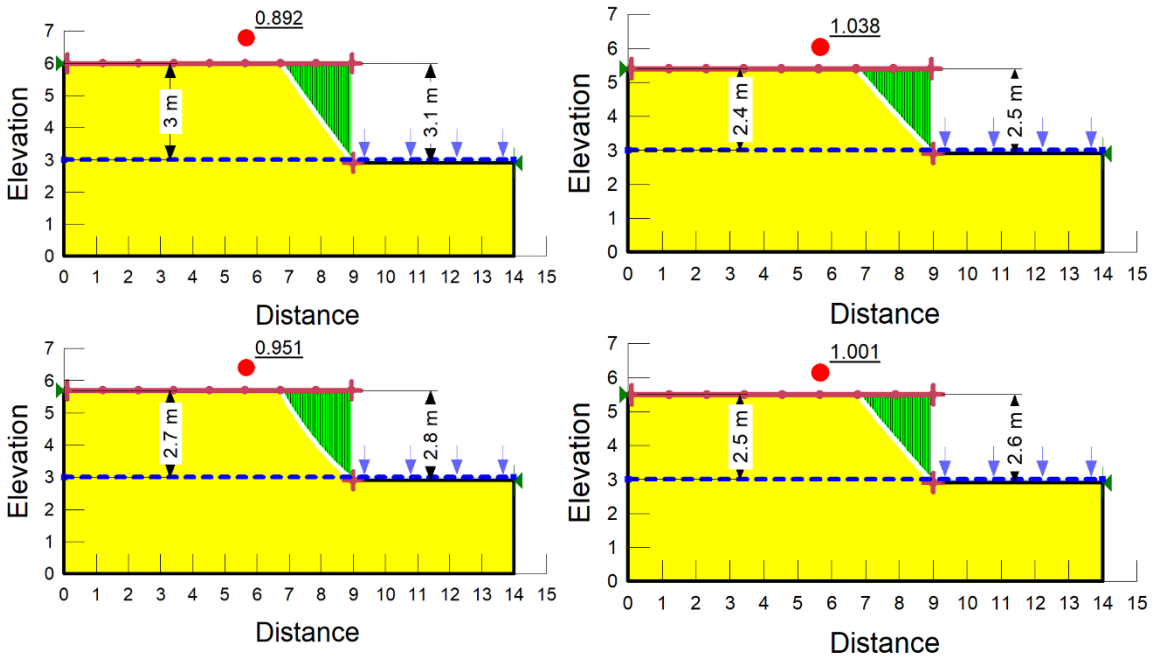

Figure 4.6. Determination of critical height using SLOPE/W.

Step 2: Simulation of Rainfall Event

Once the critical height is determined for a given GWT, rainfall infiltration is simulated by implementing influx boundary conditions along the ground surface in SEEP/W (Figure 4.7). To represent the worst-case scenario, the seepage analyses employed the maximum precipitation rate aligned with the saturated hydraulic conductivity value (See Table 4.1). Furthermore, it was assumed that there would be no accumulation of excess rainfall on the ground surface (i.e., runoff).

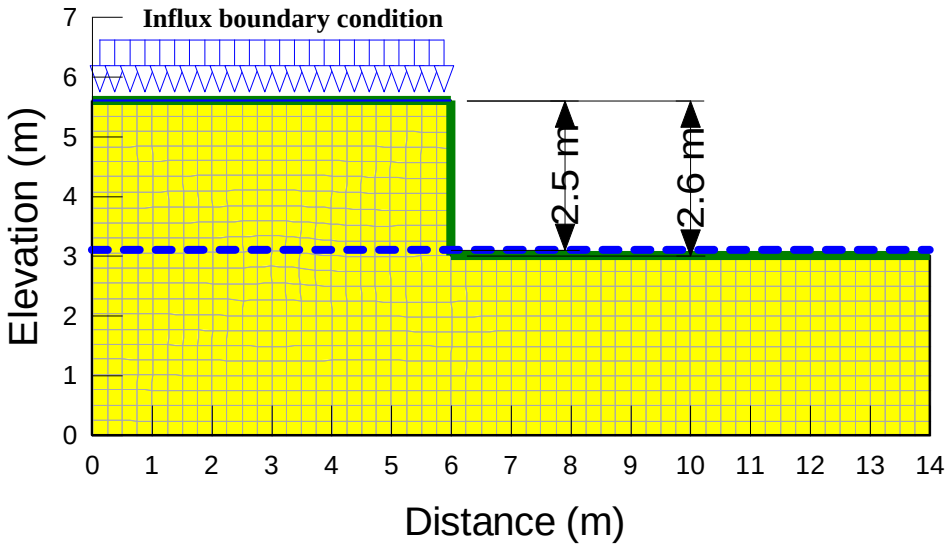

Figure 4.7. Application of influx boundary conditions to simulate rainfall infiltration.

Step 3: Determination of active earth pressure distribution and resultant force

For each time step of seepage analyses, pore-water distribution profile is determined. This information is then used to calculate positive and negative active earth pressure distribution using Eq. (3.8) , as illustrated in Figure 4.8. Examining the non-linear active earth pressure distribution line requires subdividing the area into smaller, manageable sections to determine positive and negative regions accurately. This is achieved by dividing the area into equal parts and then calculating the area of each part using the formula for the area of a trapezoid. For example, as depicted in Figure 4.8, four trapezoid shapes (A_1 to A_4) and one triangle (A_5) can be seen in the negative earth pressure distribution. Adding up the areas of these shapes yields the stabilizing force (indicated by the red arrow). Similarly, determining the destabilizing forces involves adding the area of the positive triangle (A_6)

and trapezoids (A_7 to A_{11}) (shown by the blue arrow). Ultimately, subtracting the destabilizing forces from the stabilizing forces results in the required resultant force (depicted by the yellow arrow), ensuring trench stability. Over time, the negative area experiences a progressive reduction due to the decline in matric suction associated with the rainfall event, leading to an amplified instability of the UVT.

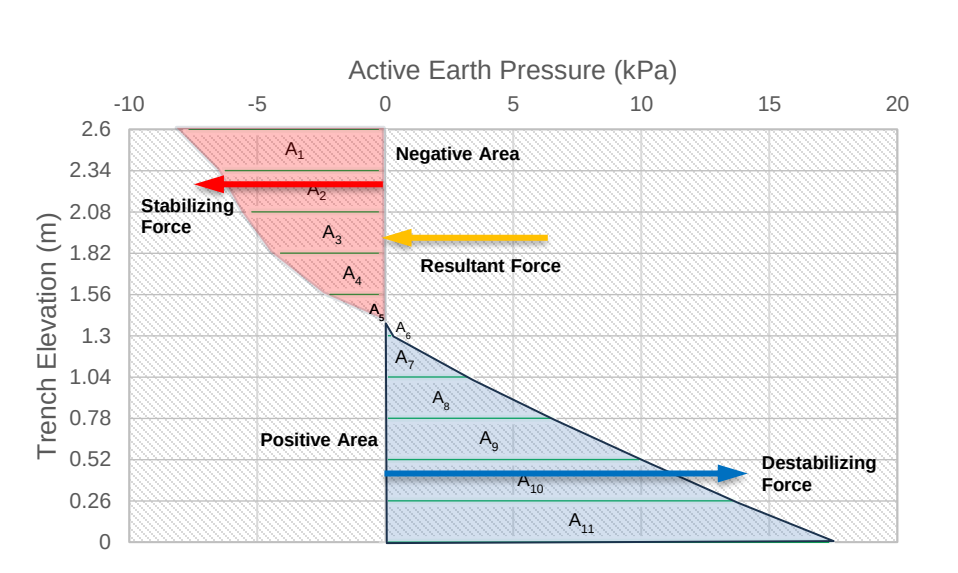

Figure 4.8. Example of active earth pressure distribution in a UVT based on the negative and positive pore-water pressure distribution. The red and blude area indicate stabilizing and destabilizing force, respectively.

Step 4: Determination of optimum depth of resultant force

As mentioned earlier, the primary objective of this study is to optimize the enhancement of the FOS by applying the resultant force to various depths within the UVT. To achieve this goal, the trench depth is evenly divided into sections, each representing a potential

point for applying the resultant force. The computed resultant force is applied at specific depths (0%, 20%, 40%, 60%, 80%, and 100% of the critical height) against the soil mass and then stability analyses are conducted using SLOPE/W to investigate FOS for each depth of resultant force application. Figure 4.9 illustrates this process for a UVT with the GWT at a depth of 3.6 m. In this specific UVT, the designated depths for applying the resultant force are 0, 0.6, 1.2, 1.8, 2.4, and 3 m relative to the trench's overall depth. After calculating FOS values for each depth, a comparison is made, identifying the depth of resultant force application that demonstrates the most substantial increase in FOS. This depth is considered the optimal depth for applying the resultant force, ensuring the highest level of enhanced stability.

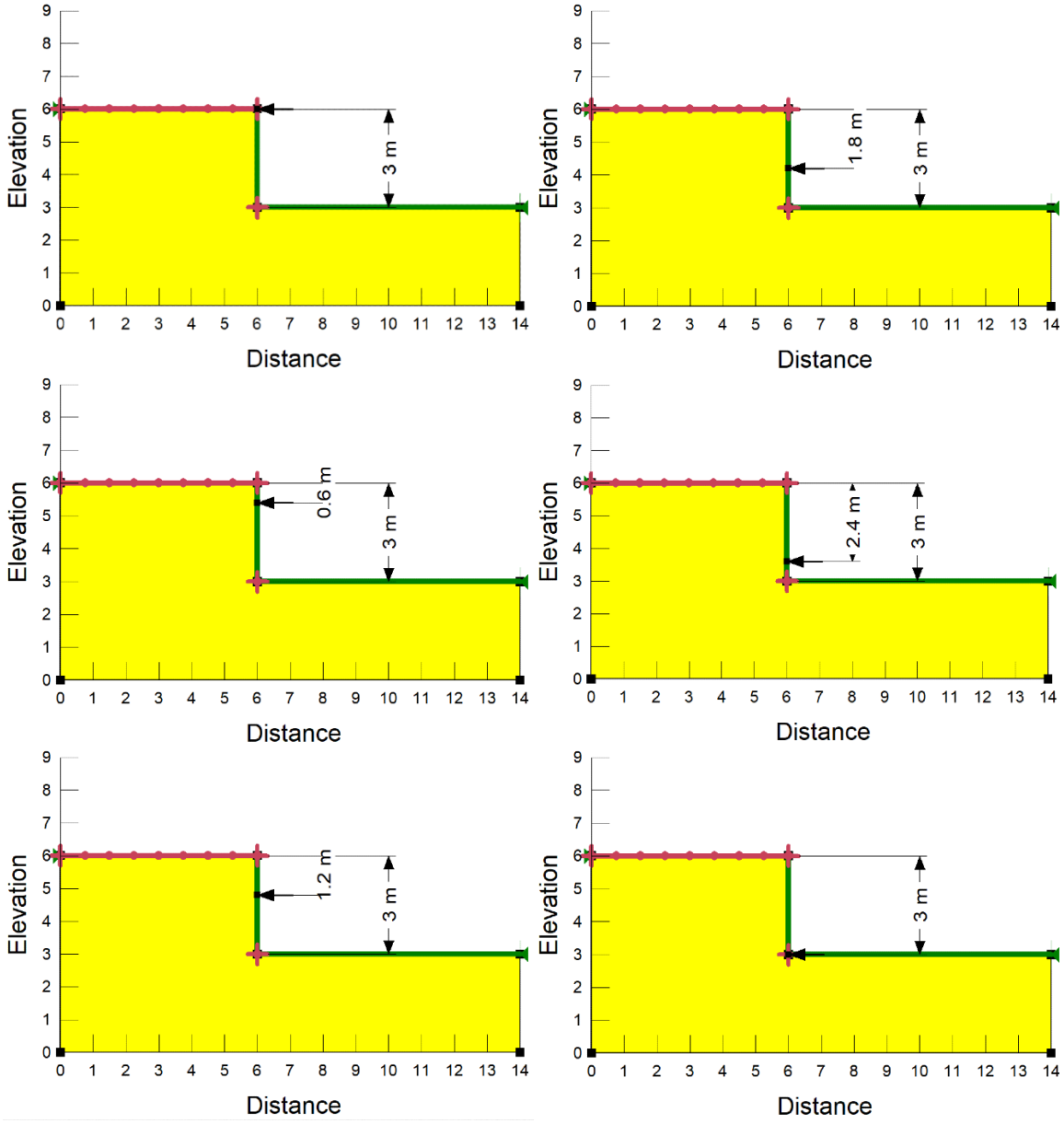

Figure 4.9. Example of the determination of the optimum depth of the resultant force by applying it at various depth of UVT.

5. ANALYSIS OF THE RESULTS

5.1 Critical Heights

As the first step, critical heights for GWT at 1.1 m (Scenario I), 1.4 m (Scenario II), 2.5 m (Scenario III), and 3.6 m (Scenario IV) were determined using SLOPE/W, shown in Figure 5.1. The critical heights were determined to be 3.3 m, 2 m, 2.6 m, and 3 m, respectively. The variation of critical height with respect to GWT is shown in Figure 5.2. This figure is generated using the GWT and critical height data from the presented scenarios, clearly demonstrating that critical height is dependent on both the trench depth and GWT. For instance, factors like hydrostatic pressure can significantly influence the critical depth. Thus, the highest critical height was obtained with the shallowest GWT (i.e., 1.1 m) due to the contribution of hydrostatic pressure within the trench towards stability.

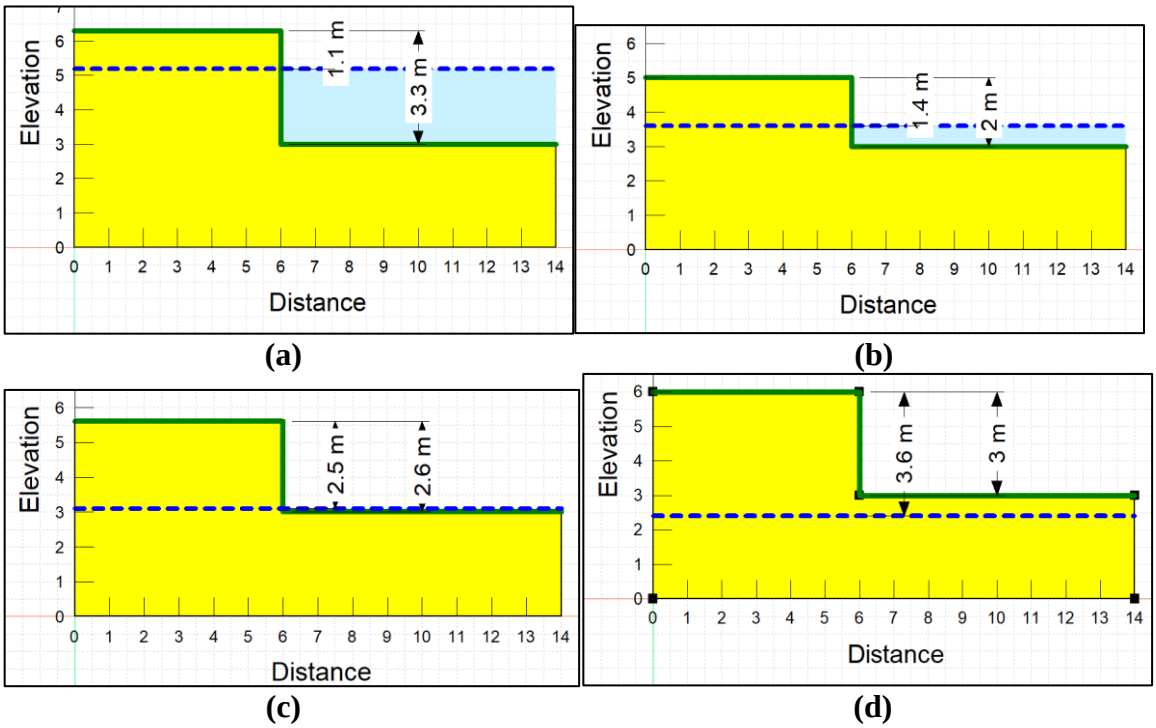

Figure 5.1. Determination of critical heights using SLOPE/W for GWT at (a) 1.1 m, (b) 1.4 m, (c) 2.5 m and (d) 3.6 m.

Understanding the critical height under various conditions is a little complicated. The complexity result from the non-linear relationship between critical height, GWT, and trench depth, as illustrated in Figure 5.2. Specifically, a substantial increase in critical height is observed when the trench depth exceeds the GWT (due to hydrostatic pressure). However, the influence of trench depth would be less noticeable when it is below the GWT. Therefore, extrapolating a comprehensive curve for various GWT and trench depths becomes a challenging task due to these complex conditions. Notably, Richard et al. 2021 have determined this relationship using Extended Rankine theory for the soil employed in this study and a fixed trench depth. For the purpose of comparison, FOS for each scenario was calculated using Eq. (3.8) and based on the active earth pressure profile to see if FOS is close to unity for the initial condition (i.e., critical height). Active earth pressure profiles for the four different scenarios are shown in Figure 5.3, which were in turn used to calculate FOS as summarized in Table 5.1, where, P_1 shows the resistance force and P_2 represents the driving force. The FOS values calculated analytically were close to the unity, which indicates that the difference in critical heights obtained from both numerical (i.e., SLOPE/W) and analytical (i.e., Eq. (3.8)) analyses are not remarkable.

Table 5.1. Summary of active thrusts and FOS for different scenarios.

Scenario	P_1	P_2	D_w [a)]	P_w [b)]	FOS [c)]
I	5.03	29.55	2.2	23.71	0.97
II	6.06	6.48	0.6	1.76	1.2
III	9.24	10.93	0.1	0.05	0.85
IV	11.24	12.75	-	-	0.88

[a)] Distance from the GWT to the bottom of the trench (= critical height – depth of GWT)
[b)] force due to the hydrostatic pressure (in case the bottom of the trench is below the GWT)
[c)] $(P_1 + P_w)/P_2$

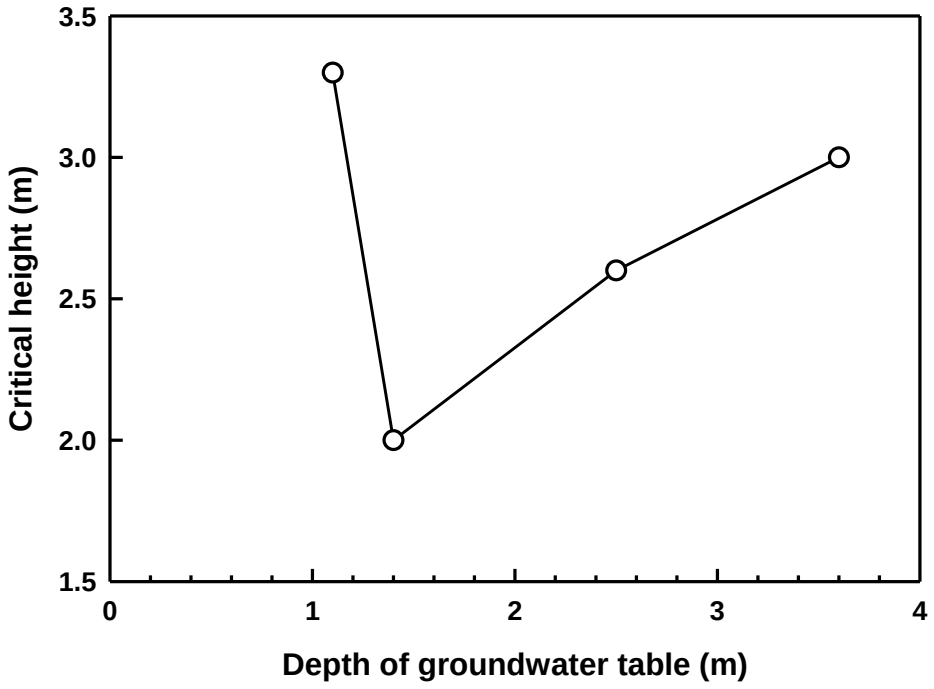

Figure 5.2. Variation of critical height with respect to depth of GWT.

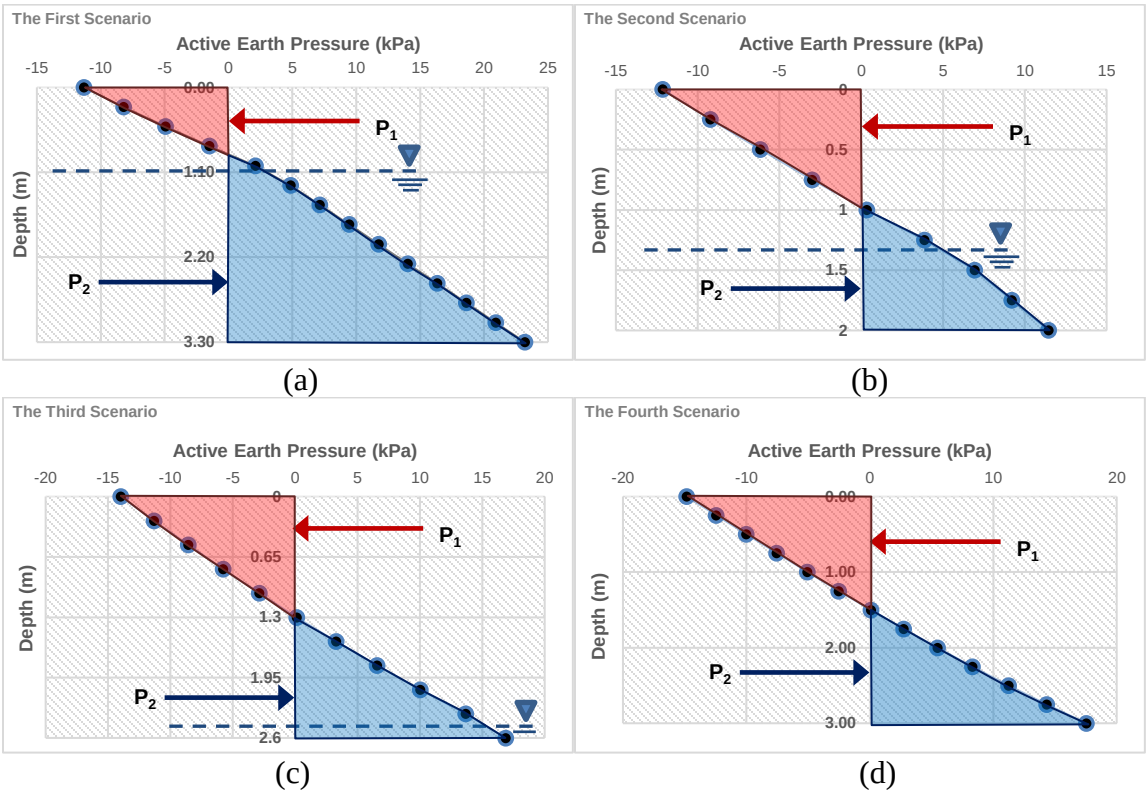

Figure 5.3. Active earth pressure profile for GWT at (a) 1.1 m (Scenario I), (b) 1.4 m (Scenario II), (c) 2.5 m (Scenario III) and (d) 3.6 m (Scenario IV).

5.2 Resultant Force under Rainfall Event

As discussed earlier, the resultant force is determined by calculating the difference between the negative (stabilizing) and positive (destabilizing) active thrusts. In cases where the GWT is above the bottom of UVT, the water is pumped out to create dry working conditions in practice. However, the water level within the UVT may not quickly rebound if the soil has low permeability. Hence, in this report, the contribution of hydrostatic pressure within UVTs towards negative active thrust was neglected in calculating the resultant force for conservative analysis. The variation of pore-water pressure, active earth pressure and resultant force with time for each scenario is as follows:

Scenario I

Based on the seepage analysis conducted with SEEP/W, the UVT reached near saturation after 3 days of the onset of rainfall infiltration. Figure 5.4 depicts the profile of pore-water pressure following continuous days of rainfall for this scenario. Certainly, approaching the vertical zero line in this figure indicates a diminishing impact of matric suction and suction stress. This reduction is attributed to the infiltration of rainfall into the unsaturated soil. Also, the variation of the active earth pressure profile with time is shown in Figure 5.5. Same as the pore-water pressure rainfall infiltration and reduction in suction stress led to a reduction of active earth pressure. Table 5.2 summarizes FOS and resultant force for different time steps under rainfall event. The resultant force for the three days of rainfall varied between 24.5 kN/m and 26.8 kN/m.

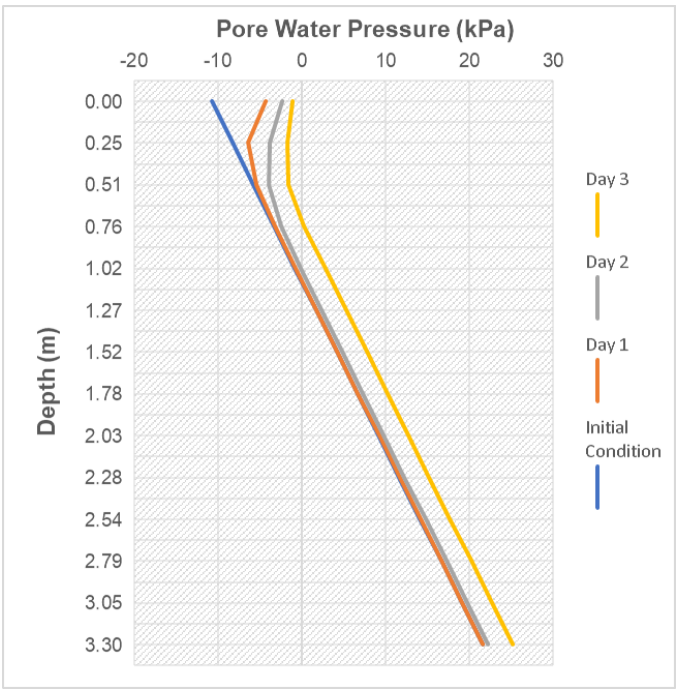

Figure 5.4. Variation of pore-water pressure with time for the UVT in Scenario I (GWT at 1.1 m).

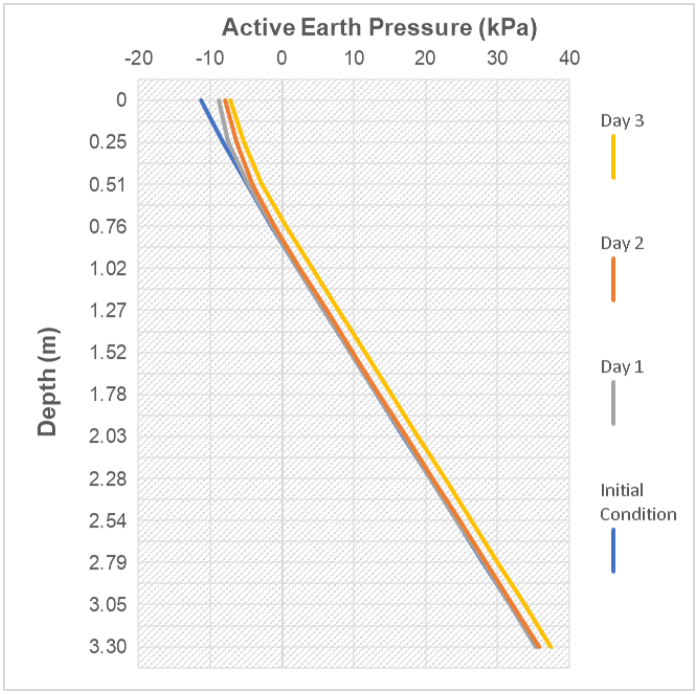

Figure 5.5. Variation of active earth pressure with time for the UVT in Scenario I (GWT at 1.1 m).

Table 5.2. Variation of FOS and resultant force with time under rainfall event (Scenario I).

Time (days)	Initial	1	2	3
FOS	1	0.957	0.888	0.812
Resultant Force (kN/m)	24.52	25.13	25.92	26.85

Scenario II

Based on the seepage analysis conducted with SEEP/W, the UVT reached near saturation after 5 days of the onset of rainfall infiltration (Figure 5.6). The variation of the active earth pressure profile with time is shown in Figure 5.7. Table 5.3 summarizes FOS and resultant force for different time steps under rainfall event. The resultant force for the three days of rainfall varied between 0.4 kN/m to 3.9 kN/m.

Table 5.3. Variation of FOS and resultant force with time under rainfall event (Scenario II).

Time (days)	Initial	1	2	3	4	5
FOS	1	0.997	0.975	0.952	0.928	0.922
Resultant Force (kN/m)	0.426	0.901	1.455	2.104	2.904	3.902

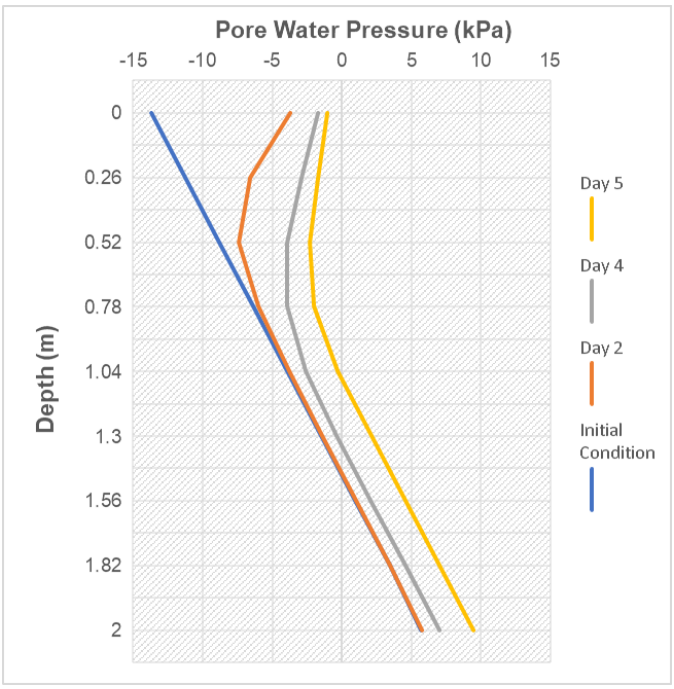

Figure 5.6. Variation of pore-water pressure with time for the UVT in Scenario II (GWT at 1.4 m).

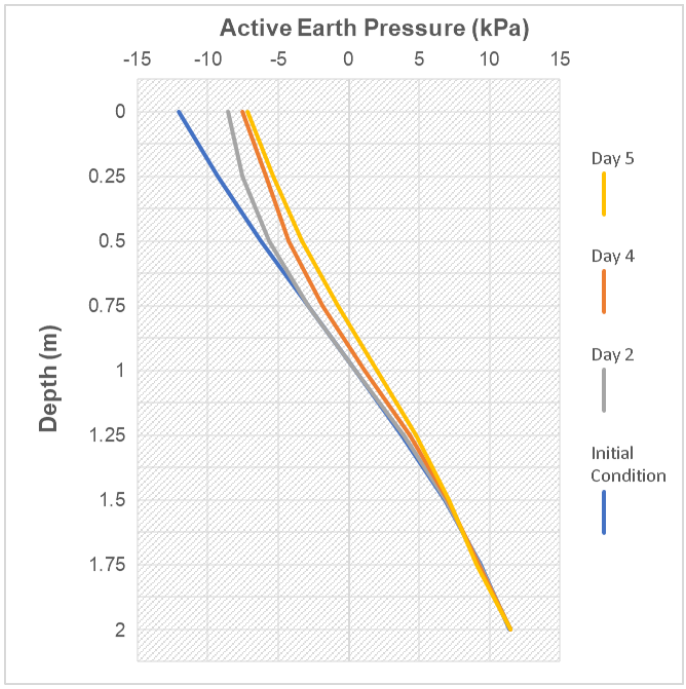

Figure 5.7. Variation of active earth pressure with time for the UVT in Scenario II (GWT at 1.4 m).

Scenario III

Based on the seepage analysis conducted with SEEP/W, the UVT reached near saturation after 17 days of the onset of rainfall infiltration (Figure 5.8). The variation of the active earth pressure profile with time is shown in Figure 5.9. Table 5.4 summarizes FOS and resultant force for different time steps under rainfall events. The resultant force for the three days of rainfall varied between 1.75 kN/m to 12.7 kN/m.

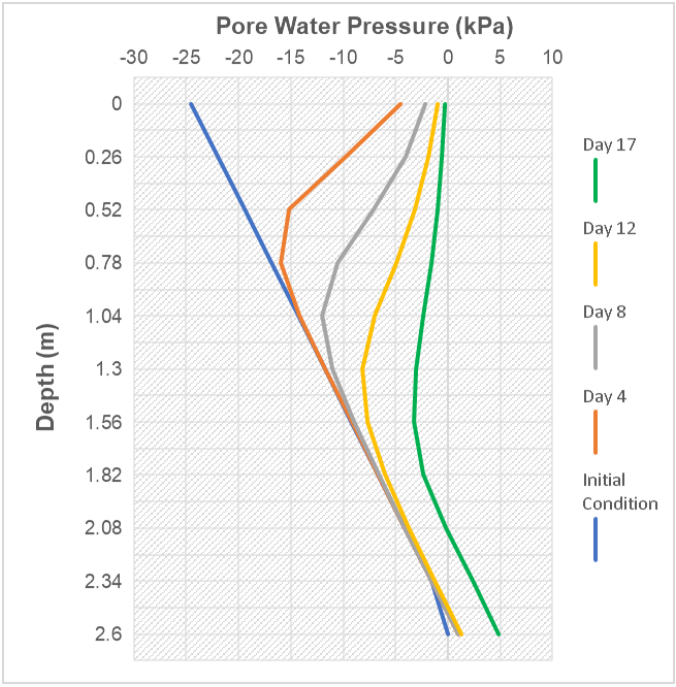

Figure 5.8. Variation of pore-water pressure with time for the UVT in Scenario III (GWT at 2.5 m).

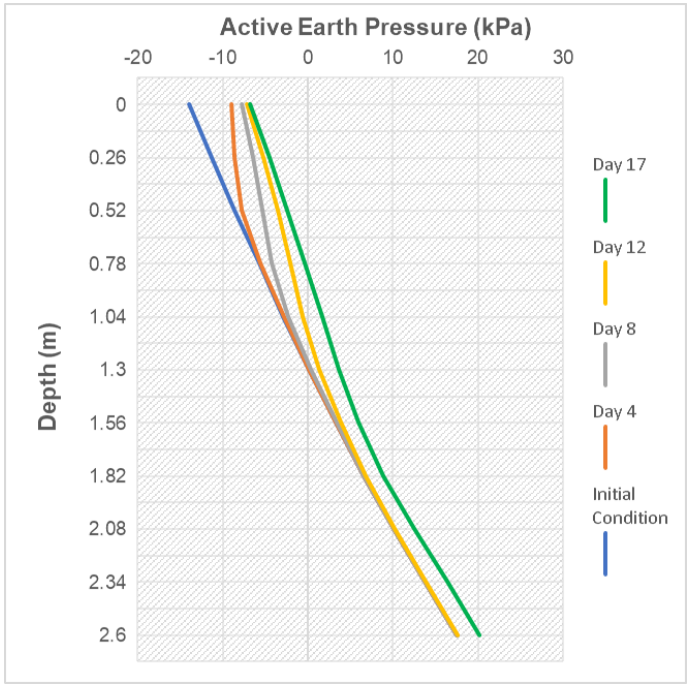

Figure 5.9. Variation of active earth pressure with time for the UVT in Scenario III (GWT at 2.5 m).

Table 5.4. Variation of FOS and resultant force with time under rainfall event (Scenario III).

Time (days)	Initial	1	2	3	4	5	6	7	8	9
FOS	1	0.991	0.982	0.972	0.962	0.952	0.941	0.929	0.918	0.906
Resultant Force (kN/m)	1.76	2.13	2.55	2.96	3.39	3.84	4.30	4.77	5.26	5.78
Time (days)	10	11	12	13	14	15	16	17		
FOS	0.893	0.88	0.867	0.852	0.837	0.82	0.803	0.787		
Resultant Force (kN/m)	6.333	6.94	7.61	8.38	9.16	10.04	11.15	12.69		

Scenario IV

Based on the seepage analysis conducted with SEEP/W, the UVT reached near saturation after 35 days of the onset of rainfall infiltration (Figure 5.10). The variation of the active earth pressure profile with time is shown in Figure 5.11. Table 5.5 summarizes FOS and resultant force for different time steps under rainfall events. The resultant force for the three days of rainfall varied between 1.5 kN/m to 19.2 kN/m.

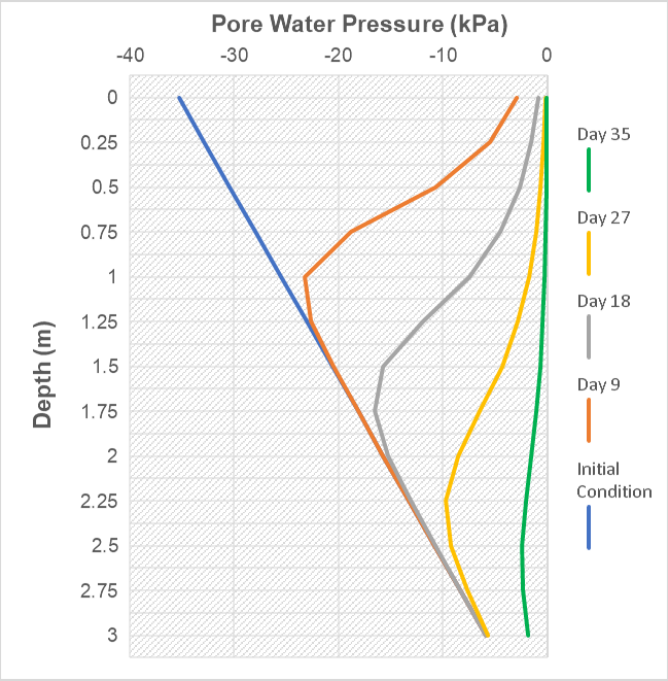

Figure 5.10. Variation of pore-water pressure with time for the UVT for Scenario IV (GWT at 3.6 m).

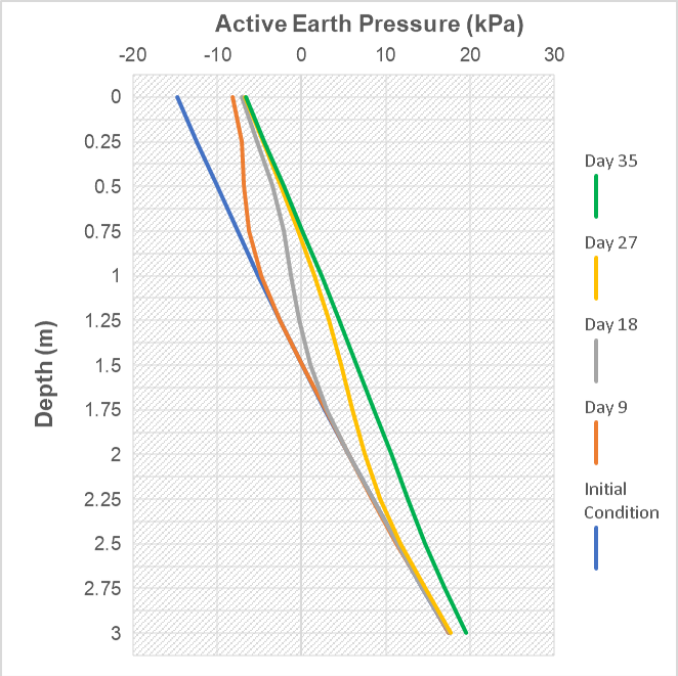

Figure 5.11. Variation of active earth pressure with time for the UVT in Scenario IV (GWT at 3.6 m).

Table 5.5. Variation of FOS and resultant force with time under rainfall event (Scenario IV)

Time (days)	Initial	3	6	9	12	15	18	21	24
FOS	1	0.98	0.958	0.935	0.911	0.886	0.859	0.831	0.802
Resultant Force (kN/m)	1.513	2.484	3.611	4.852	6.181	7.583	9.096	10.714	12.403

Time (days)	27	30	33	35
FOS	0.771	0.739	0.707	0.684
Resultant Force (kN/m)	14.166	16.002	17.875	19.215

In all scenarios, the resultant force steadily rises as rainfall infiltration persists, owing to the reduction in the negative active thrust until the unsaturated layer becomes completely saturated. The highest resultant forces were observed for Scenario I since the hydrostatic pressure within the UVTs was neglected in calculating the resultant forces. Scenario I also showed the minimum range of resultant force because the UVT became close to fully saturation in a short period of time due to the shallow GWT. Apart from this scenario, it can be seen that the maximum resultant force increases with an increase in the depth of GWT.

5.3 Application of Resultant Force against UVT

For each time step, the calculated resultant forces were applied against UVTs to investigate their impact on FOS at the depths of 0%, 20%, 40%, 60%, 80%, and 100% from the ground surface. Analyzing the depth and FOS data for continuous rainfall events following the application of resultant forces leads to the identification of trends. This comprehensive assessment allows for the creation of a trendline, identifying the optimal areas for applying resultant forces. The results for Scenario I, II, III, and IV are shown in Figure 5.12, Figure 5.13, Figure 5.14, and Figure 5.15, respectively.

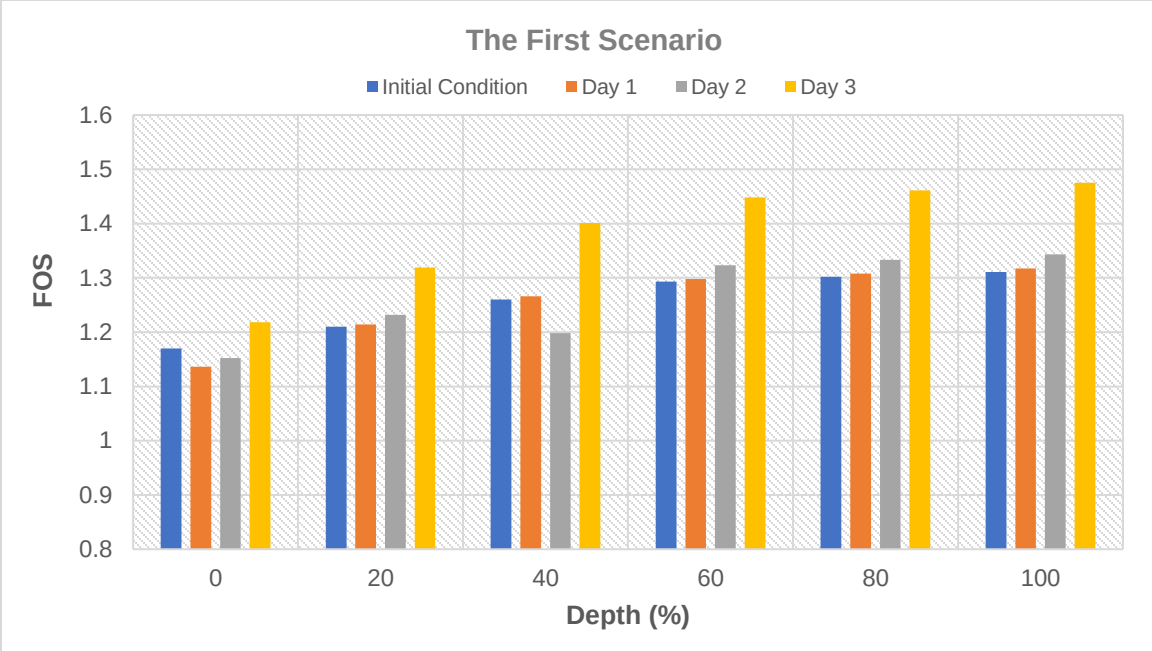

Figure 5.12. Variation of FOS for different depth of resultant force application (Scenario I, GWT at 1.1 m) during rainfall infiltration.

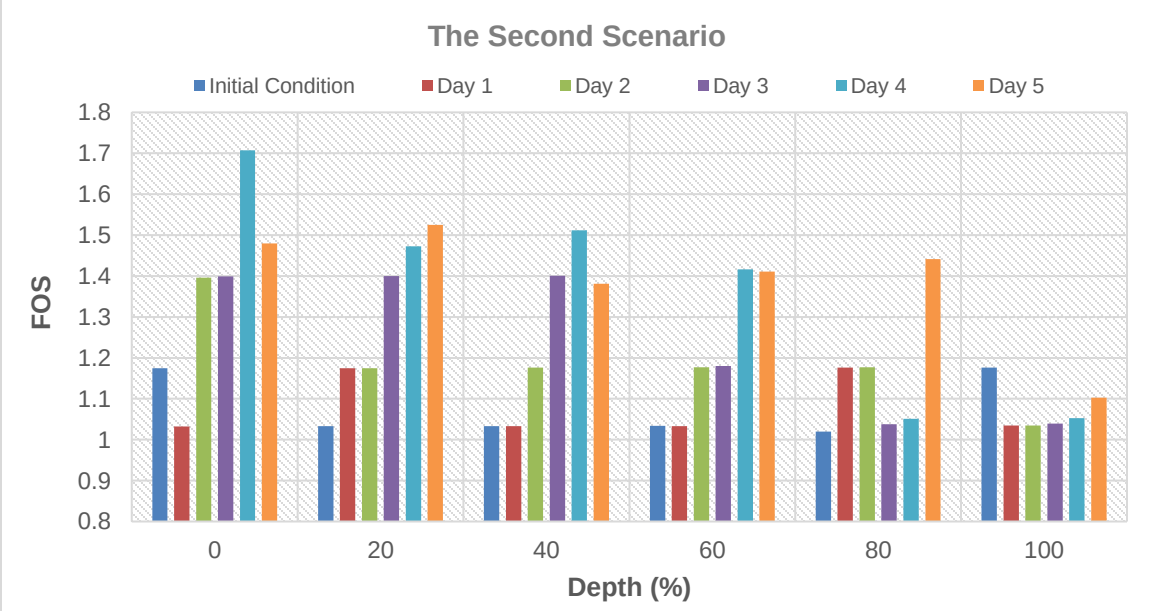

Figure 5.13. Variation of FOS for different depth of resultant force application (Scenario II, GWT at 1.4 m) during rainfall infiltration.

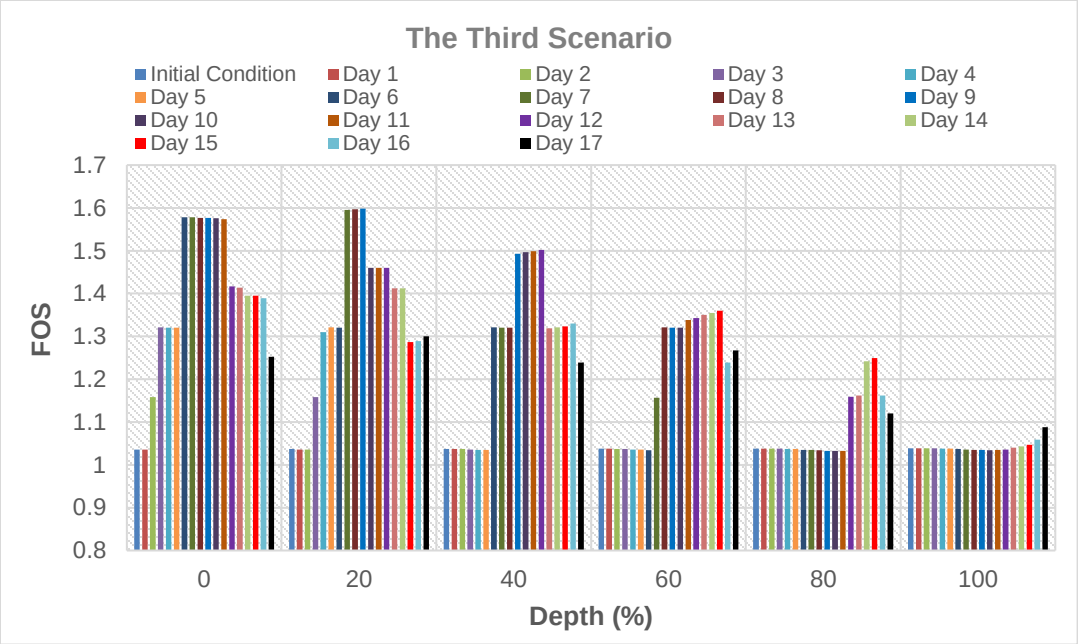

Figure 5.14. Variation of FOS for different depth of resultant force application (Scenario III, GWT at 2.5 m) during rainfall infiltration.

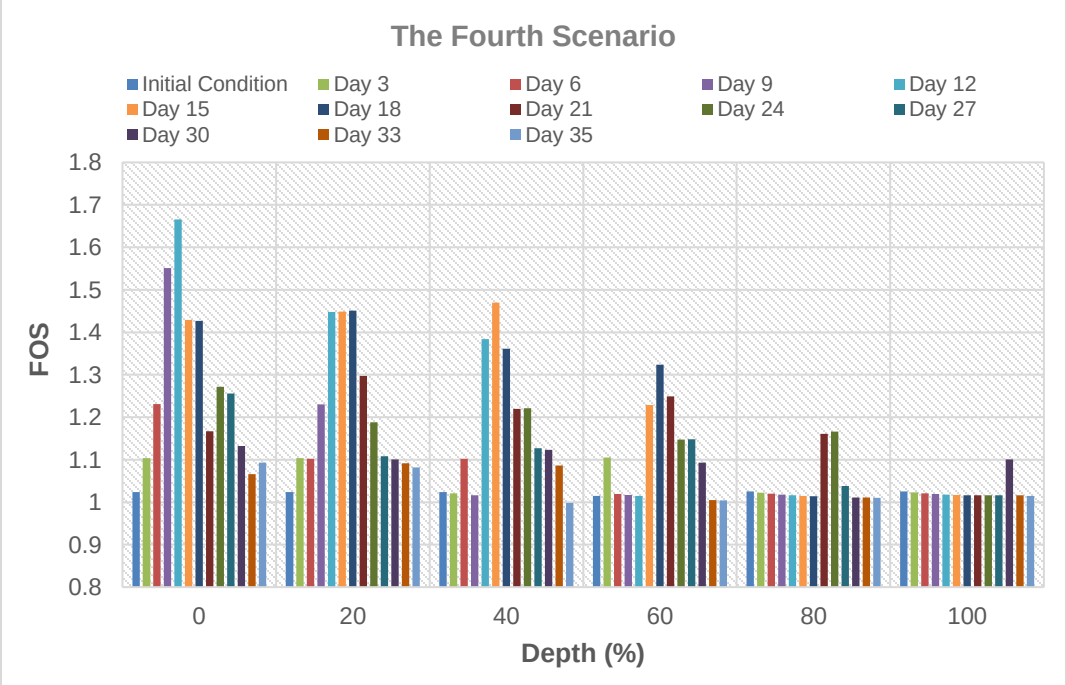

Figure 5.15. Variation of FOS for different depth of resultant force application (Scenario IV, GWT at 2.5 m) during rainfall infiltration.

For Scenario I, the application of resultant force increased FOS greater than the minimum acceptable value (i.e., 1.2) except for the application at the top of UVT (i.e., 0%). This is because, from the beginning, the resultant forces were overestimated by neglecting the hydrostatic pressure within the UVTs. No significant changes in FOSs were observed with time for the application depths greater than 60%; however, overall, FOSs increased with time as the application depth got deeper. On the other hand, for Scenario III and IV, FOS gradually increases up to a certain time step and then starts decreasing as UVTs reach the saturated condition for each application depth except for 100%. This means that the effectiveness of the application of resultant force reduces as soil suction within UVTs significantly decreases even though the estimated resultant force becomes maximized. This phenomenon led to the minimum FOSs when UVTs reached saturation due to a relatively higher loss in soil suction compared to other scenarios. It is interesting to note that Scenario II shows the mixed behaviours of Scenario I and Scenario III/IV.

It turned out that, for Scenarios III and IV, applying the resultant forces at depths deeper than 80% is not effective throughout rainfall duration. This means that the analytically estimated resultant forces are not high enough to increase FOS greater than 1.2.

5.4. Determination of Optimum Resultant Force and Application Depth

The result in Section 5.3 indicates that the application of resultant force can improve the stability of UVTs remarkably. However, FOSs for the early stage are less than 1.2 (except Scenario I) since UVTs were excavated up to the critical heights with FOS close to 1.0. Hence, in this section, additional analyses are carried out to determine the most efficient resultant force and application depth that can lead to FOS higher than 1.2 throughout the

raining duration. As mentioned earlier, it is not effective to apply the resultant forces at depths deeper than 80% throughout rainfall duration. Furthermore, the application of a resultant force at the top of UVTs is not feasible due to the potential for passive failure. From a geotechnical perspective, placing a resultant force beyond a depth of 60% can also impede fieldwork. Hence, in this section, analyses were conducted assuming the resultant forces are applied at a depth of 20% and 40% of the height of UVT.

The analysis results for Scenario I, II, III, and IV are summarized in Table **5.6**, Table **5.7**, Table **5.8**, and Table **5.9**. FOSs higher than 1.2 are highlighted in gray. Three resultant forces were considered in the analyses, which include minimum (i.e., resultant force for initial condition), maximum (i.e., resultant force for the last time step), and median. As expected, for Scenario I, FOSs are greater than 1.2 for all cases since FOS for the initial condition was close to 1.2 by neglecting the hydrostatic pressure within the UVT. For Scenarios II and III, the application of the median value of resultant force kept the UVTs stable for the entire rainfall duration. FOSs for Scenario IV drops below the required FOS (i.e., 1.2) 21 days after the start of rainfall; however, since UVTs are excavated for a temporary purpose, it can be assumed that application of the median value of resultant force can keep UVTs stable during the construction object. These observations indicate that it is the most practical and economical to apply the median value of resultant force at the depth of 20% or 40% to maintain UVTs stable considering rainfall infiltration.

Table 5.6. Variation of FOS due to the application of resultant force at 20% and 40% of the height of UVT (Scenario I).

Scenario I (GWT at 1.1 m)						
DAYS	Location					
	40%			20%		
	Load (kN/m)					
	24.52 (Min)	25.61 (Median)	26.85 (Max)	24.52 (Min)	25.61 (Median)	26.85 (Max)
	FOS					
0	1.26	1.29	1.32	1.21	1.23	1.25
1	1.25	1.28	1.21	1.20	1.22	1.24
2	1.16	1.19	1.22	1.21	1.23	1.25
3	1.25	1.37	1.40	1.27	1.29	1.32

Table 5.7. Variation of FOS due to the application of resultant force at 20% and 40% of the height of UVT (Scenario II).

GWT = 1.4 m						
DAYS	Location					
	40%			20%		
	Load (kN/m)					
	0.43 (Min)	1.95 (Median)	3.90 (Max)	0.43 (Min)	1.95 (Median)	3.90 (Max)
	FOS					
0	1.03	1.24	1.83	1.03	1.46	1.82
1	1.00	1.22	1.81	1.01	1.44	1.81
2	0.98	1.42	1.83	0.99	1.42	1.80
3	0.96	1.39	1.81	0.97	1.39	1.78
4	0.95	1.37	1.55	0.95	1.37	1.75
5	0.94	1.48	1.38	0.94	1.47	1.53

Table 5.8. Variation of FOS due to the application of resultant force at 20% and 40% of the height of UVT (Scenario III)

GWT = 2.6 m						
DAYS	Location					
	40%			20%		
	Load (kN/m)					
	1.76 (Min)	6.06 (Median)	12.69 (Max)	1.76 (Min)	6.06 (Median)	12.70 (Max)
	FOS					
0	1.03	1.43	1.87	1.04	1.83	1.81
1	1.03	1.42	1.86	1.03	1.82	1.80
2	1.02	1.41	1.86	1.02	1.65	1.80
3	1.01	1.40	1.85	1.01	1.65	1.79
4	1.00	1.39	1.84	1.00	1.64	1.79
5	0.99	1.66	1.84	0.99	1.64	1.78
6	0.98	1.65	1.63	0.98	1.63	1.77
7	0.97	1.64	1.66	0.97	1.62	1.76
8	0.95	1.51	1.61	0.95	1.61	1.58
9	0.94	1.50	1.60	0.94	1.60	1.56
10	0.93	1.49	1.45	1.05	1.46	1.56
11	0.92	1.48	1.44	1.04	1.45	1.54
12	0.90	1.47	1.43	1.03	1.44	1.53
13	0.89	1.37	1.42	1.01	1.43	1.51
14	0.87	1.26	1.40	1.00	1.41	1.35
15	0.85	1.24	1.38	0.98	1.33	1.34
16	0.84	1.22	1.37	0.96	1.20	1.32
17	0.82	1.20	1.24	0.82	1.18	1.30

Table 5.9. Variation of FOS due to the application of resultant force at 20% and 40% of the height of UVT (Scenario IV)

DAYS	GWT = 3.6 m					
	Location					
	40%			20%		
	Load (kN/m)					
	1.51 (Min)	9.67 (Median)	19.22 (Max)	1.51 (Min)	9.67 (Median)	19.22 (Max)
	FOS					
0	1.02	1.83	2.02	1.02	1.86	2.04
3	1.00	1.82	1.76	1.01	1.77	1.90
6	0.98	1.55	1.74	0.98	1.76	1.68
9	0.96	1.54	1.73	0.96	1.75	1.66
12	0.94	1.52	1.56	0.93	1.50	1.64
15	0.91	1.51	1.53	0.91	1.48	1.35
18	0.88	1.37	1.39	0.88	1.46	1.28
21	0.85	1.30	1.26	0.85	1.31	1.31
24	0.82	1.18	1.15	0.82	1.25	1.14
27	0.79	1.15	1.11	0.79	1.13	1.10
30	0.76	1.12	1.07	0.76	1.09	1.06
33	0.73	1.08	1.03	0.73	1.06	1.02
35	0.70	1.05	1.00	0.70	1.12	1.08

6. CONCLUSIONS AND FUTURE WORKS

In this report, a methodology is proposed to improve the stability of UVT by applying a load against the UVT considering the rainfall events. For this, comprehensive numerical analyses were carried out using numerical modeling geotechnical software, SEEP/W and SLOPE/W (GeoStudio 2002). Several scenarios with varying GWT depths and subsequent critical heights of UVTs were considered in the numerical analyses to estimate the optimum load and its location to increase FOS of UVTs from the practical and economical point of view. The conclusions drawn from the analyses are as follows:

- The critical height of UVT is affected by not only the matric suction distribution profile but also the level of groundwater within the UVT. Due to this reason, the critical height of a UVT with a shallow GWT can be higher than that of a UVT with a deeper GWT. This is attributed to the effect of hydrostatic pressure against the UVTs.
- The study successfully determined the resultant force by considering positive and negative active thrusts. The application of resultant forces at different depths within the UVT was analyzed, leading to insights into the variation of FOS during rainfall events.
- FOS of a UVT continuously changes depending on the magnitude of the resultant force and the depth of its application during rainfall events. Hence, it is strongly suggested that comprehensive numerical analyses be carried out to investigate the variation of FOS to determine the worst-case scenario.
- The effectiveness of the application of resultant force against the UVT reduces as soil suction within the UVT decreases even though the estimated resultant force becomes maximized as the UVT reaches saturated condition.

- Utilizing the median resultant force value at depths corresponding to either 20% or 40% of the critical height of UVT is the most practical approach considering rainfall events.
- The proposed approach involves applying a load against the UVT to enhance stability during rainfall events. The analysis suggests that placing resultant forces at an optimum depth of the UVT can effectively improve stability. This offers a practical and economical method for safe trenching operations, potentially mitigating the need for trench boxes.

The numerical modeling approach used in this study provides valuable insights into the stability of UVT during rainfall infiltration, aiding in trench design considerations and safety assessments. This report contributes to the understanding of trench stability and provides useful guidelines for optimizing the point of load placement and the corresponding load value to maintain the stability of UVTs under the influence of rainfall infiltration. The findings in this report can be utilized to improve trench design practices and ensure the safety of such structures in real-world construction scenarios.

The results in this report were obtained based on the limited levels of GWT and the rainfall intensity. Hence, more research is necessary taking account of variations in soil characteristics, diverse trench geometries, and the impact of varying GWT depths. A thorough investigation of these elements will provide engineers and geotechnical experts with a more profound comprehension of the intricate correlation between the active earth pressure and the extension of trench excavation depth. This, in turn, can contribute to the

development of more resilient design guidelines and enhanced safety measures for UVTs in regions prone to rainfall infiltration.

7. REFERENCES

Bishop, A.W. 1959. The principle of effective stress. Teknisk ukeblad 106(39), 859–863.

Bishop, A.W. and Bjerrum, L. 1960. The relevance of the triaxial test to the solution of stability problems. ASCE Conf. on Strength of Cohesive Soils, Norwegian Geotechnical Institute Publication: 437-501.

Brooks, R. and Corey, A. 1964. Hydraulic properties of porous media. Hydrology Paper No. 3. Civil Engineering Department, Colorado State University, Fort Collins, CO.

Fredlund, D., Xing, A. and Huang, S. 1994. Predicting the permeability function for unsaturated soils using the soil-water characteristic curve. Canadian Geotechnical Journal 31(4): 533–546.

Fredlund, D.G. and Rahardjo, H. 1993. Soil Mechanics for Unsaturated Soils. John Wiley & Sons.

Fredlund, D.G. and Xing, A. 1994. Equations for the soil-water characteristic curve. Canadian Geotechnical Journal 31(4): 521–532.

Jannadi, O.A. 2008. Risks associated with trenching works in Saudi Arabia. Building and Environment 43(5): 776–781.

Karube, D. and Kato, S. 1994. An ideal unsaturated soil and the Bishop's soil. In Proceedings of the 13th International Conference on Soil Mechanics and Foundation Engineering: 43–46.

Karube, D. and Kawai, K. 2001. The role of pore water in the mechanical behavior of unsaturated soils. Geotechnical and Geological Engineering 19: 211–241.

Krishnapillai, S.H. and Ravichandran, N. 2012. New soil-water characteristic curve and its performance in the finite-element simulation of unsaturated soils. International Journal of Geomechanics 12(3): 209–219.

Lu, N., Godt, J.W. and Wu, D.T. 2010. A closed-form equation for effective stress in unsaturated soil. Water Resources Research 46, W05515: 1–14.

Lu, N. and Likos, W.J. 2004. Unsaturated Soil Mechanics, John Wiley&Sons. Inc., Hoboken, USA.

Lu, N. and Likos, W.J. 2006. Suction stress characteristic curve for unsaturated soil. Journal of Geotechnical and Geoenvironmental Engineering 132(2): 131–142.

Nishimura, T., Toyota, H., Vanapalli, S. and Oh, W.T. 2008. Determination of the shear strength behavior of an unsaturated soil in the high suction range using vapor pressure technique. In Proceedings of the 1st European Conference on Unsaturated Soils. Unsaturated Soils: Advances in Geo-Engineering, Toll et al. (eds). CRC Press: Taylor and Francis Group: 441-447. .

Bajestani, M.S. and Oh, W.T. 2022. Influence of soil-water characteristic curve on the safe height and stand-up time of unsupported vertical trenches in unsaturated soils. International Journal of Geotechnical Engineering 16(10): 1179-1190.

Oh, W.T. and Vanapalli, S.K. 2013. Interpretation of the bearing capacity of unsaturated fine-grained soil using the modified effective and the modified total stress approaches. International Journal of Geomechanics 13(6): 769–778.

Oh, W.T. and Vanapalli, S.K. 2010. Influence of rain infiltration on the stability of compacted soil slopes. Computers and Geotechnics 37(5): 649–657.

Oh, W.T., Vanapalli, S.K. and Puppala, A.J., 2009. Semi-empirical model for the prediction of modulus of elasticity for unsaturated soils. Canadian Geotechnical Journal 46(8): 903–914.

OSHA, 2022. Alarming rise in trench-related fatalities. https://www.osha.gov/news/newsreleases/national/07142022

Philips, Z., 2023. 2022 was a bad year for trench deaths. This year could be worse. Construction Dive. https://www.constructiondive.com/news/trench-deaths-OSHA-2022-trends/641593/

Pufahl, D., Fredlund, D. and Rahardjo, H. 1983. Lateral earth pressures in expansive clay soils. Canadian Geotechnical Journal 20(2): 228–241.

Rankine, W.J.M. 1857. On the stability of loose earth. Philosophical transactions of the Royal Society of London: 9–27.

Richard, A., Oh, W.T. and Brennan, G. 2021. Estimating critical height of unsupported trenches in vadose zone. Canadian Geotechnical Journal 58(1): 66–82.

Shahrokhabadi, S., Vahedifard, F., Ghazanfari, E. and Foroutan, M. 2019. Earth pressure profiles in unsaturated soils under transient flow. Engineering Geology 260, 105218.

Terzaghi, K. 1943. Theoretical Soil Mechanics, John Wiley & Sons, New York.

Vahedifard, F., Leshchinsky, B.A., Mortezaei, K. and Lu, N. 2015. Active earth pressures for unsaturated retaining structures. Journal of Geotechnical and Geoenvironmental Engineering 141(11): 1-11.

van Genuchten, M.T. 1980. A closed-form equation for predicting the hydraulic conductivity of unsaturated soils. Soil science society of America journal 44(5): 892–898.

Vanapalli, S., Fredlund, D., Pufahl, D. and Clifton, A. 1996. Model for the prediction of shear strength with respect to soil suction. Canadian Geotechnical Journal 33(3): 379–392.

Curriculum Vitae

Candidate's full name:

Ashkan Shirzadi

Universities attended (with dates and degrees obtained):

M.Sc.E (Drilling Engineering), Amirkabir University of Technology, 2020

B.Sc.E (Mining Engineering), Amirkabir University of Technology, 2017

Publications:

Mirabbasi, S. M., Ameri, M. J., Biglari, F. R., Shirzadi, A. (2020). 'Thermo-poroelastic wellbore strengthening modeling: An analytical approach based on fracture mechanics', Journal of Petroleum Science and Engineering, Volume 195, 107492, ISSN 0920-4105, https://doi.org/10.1016/j.petrol.2020.107492.

Mirabbasi, S. M., Ameri, M. J., Biglari, F. R., Shirzadi, A. (2020). 'An Analytical Poroelastic Model to Study the LCM Performance during the Wellbore Strengthening', Journal of Petroleum Geomechanics, 3(4), pp. 57-74. doi: 10.22107/jpg.2020.195093.1102

Conference Presentations:

'Geomechanical Study on Strengthening a Wellbore with Multiple Natural Fractures: A Poroelastic Numerical Simulation' in proceedings of the , 82nd EAGE Annual Conference & Exhibition, Oct 2021, Netherland. Doi: https://doi.org/10.3997/2214-4609.202011875